INITIAL INVESTIGATIONS INTO THE DAMPING CHARACTERISTICS OF WIRE ROPE VIBRATION ISOLATORS

by

M. A. Cutchins
J. E. Cochran, Jr.
K. Kumar

and

N. G. Fitz-Coy and M. L. Tinker

Aerospace Engineering Department
Auburn University, Alabama

(NASA-CR-180698) INITIAL INVESTIGATIONS INTO THE DAMPING CHARACTERISTICS OF WIRE ROPE VIBRATION ISOLATORS Final Technical Report (Auburn Univ.) 89 p CSCL 20K

N87-20569

G3/39 Unclas 45403

Auburn University
Aerospace Engineering
Technical Report 87-1

FINAL REPORT

INITIAL INVESTIGATIONS INTO THE DAMPING CHARACTERISTICS OF WIRE ROPE VIBRATION ISOLATORS

by

M. A. Cutchins
J. E. Cochran, Jr.
K. Kumar
N. G. Fitz-Coy
M. L. Tinker

Engineering Experiment Station
Auburn University, Alabama 36849

Prepared under

NASA Research Grant NAG8-532

George C. Marshall Space Flight Center
National Aeronautics and Space Administration

Auburn University

January 1987

ABSTRACT

Passive dampers composed of coils of multi-strand wire rope are investigated. Analytical results range from those produced by complex NASTRAN models to those of a Coulomb damping model with variable friction force. The latter agrees well with experiment. The Coulomb model is also utilized to generate hysteresis loops. Various other models related to early experimental investigations are described. Significant closed-form static solutions for physical properties of single-and multi-strand wire ropes are developed for certain specific geometries and loading conditions. NASTRAN models concentrate on model generation and mode shapes of 2-strand and 7-strand straight wire ropes with interfacial forces.

TABLE OF CONTENTS

TABLE OF CONTENTS (CONTINUED)

LIST OF FIGURES

LIST OF FIGURES (CONTINUED)

LIST OF TABLES

1. INTRODUCTION

Space activities have revitalized the importance of damping investigations. There has been a significant increase in the number of papers on the topic in the literature and a number of research investigations have been initiated. Long of interest to many, damping is receiving increased attention due to a variety of actual and potential applications; among them: large space structures, space structures with stringent pointing requirements, computer controlled flexible structures, flexible manufacturing systems, composite materials, swept-forward wings, SDI structural dynamics, and others.

The primary interest of this investigation centers on vibration isolators constructed of wire rope. Such isolators have been known to have good characteristics for some time, but have not been analyzed to a thorough enough degree to be yet used in space applications. This lack of analysis is at least partly due to the difficulty in modeling the dynamics of wire rope isolators.

Wire rope is, from the basic point of view, simply several strands of wire twisted, or wound, together. Some types are commonly called "cable" and are used to carry electricity, support bridges and "cable cars," raise and lower heavy loads and in many other practical ways. A less obvious, but equally important, use of wire rope is in shock and vibration isolation devices (Silverman, 1985; Gilbert, 1976). The structure of wire rope provides many interfaces at which a portion of the relative motion of strands of wire is converted by friction into

heat, thereby dissipating vibrational energy (Harris and Crede, 1976). Furthermore, the stiffness of wire rope structures can be tailored to provide support and restoring forces. Stiffness and damping are adjusted by varying wire diameter, the number of strands, pretensioning and the arrangement of lengths of the wire rope. Commonly, helical coils of ropes are fixed in clamps (see Fig. 1.1) to form individual shock and/or vibration isolators. The isolators are used to support and isolate communications equipment in vehicles which are subjected to large magnitude, short-term accelerations; i.e., "shocks." In addition to absorbing shock, the internal, or system, damping, (Silverman, 1985) of the wire rope devices provides vibrational isolation over wide ranges of frequencies and amplitudes.

The damping characteristics of wire rope and vibration isolators made from it are not well understood from the theoretical standpoint. Apparently, the design of individual isolators is accomplished by experimentation by engineers with considerable experience in applications of these devices (Silverman, 1985; Jewell, 1984). Realistic mathematical models of wire rope isolators would be useful in the design process and perhaps would allow the achievement of the confidence levels in isolator characteristics needed for more applications in which damping rates and dynamic response must be very accurately known to prevent resonance and control interaction problems.

2. DAMPING CONSIDERATIONS

Literature Discussion

Aside from the rather obvious use of isolators as passive damping devices for equipment mounting and/or isolation of rotating devices, it has been concluded (Rogers, et al., 1986, and others) that the use of passive plus active damping devices results in a reduced number of active control components and reduced energy and power requirements. A combination of the two types of damping can lead to more robust and reliable systems, and less expensive systems.

An examination of the literature concerning damping indicates the widely differing approaches to its investigation. The most significant paper in this regard which relates to wire rope damping is that by Pivovarov and Vinogradov (1985). Their study, however, was limited to excitation of straight wire rope which suspended a mass in pendulum fashion. Experimental hysteresis loops (shapes only) are given and several single nonlinear differential equations are solved in an attempt to simulate the phenomena.

The only other two items of literature found which discuss wire rope damping directly are LeKuch and Silverman (1983) in a designer notebook setting--a guide to isolator selection, and Kerley (1984) who just mentions wire rope "complex cable" arrangements as one type of passive damping device.

Several of the other literature papers, while not addressing wire rope damping at all, are very related to some of the tasks undertaken

during this research. One is the work of Badrakan (1985) dealing with separating and determining combined dampings from free vibrations. Another is the paper by Vakakis (1985) on unidirectional isolators (multiple mass, many degrees of freedom models).

Summary of Techniques

Perhaps the best source for damping considerations is the new book by Nashif, Jones, and Henderson (1985), although again, no mention of wire rope damping is made therein. Their emphasis is on single degree of freedom hysteretic, i.e., $k(1+i\eta)$, damping. A summary of their suggested methods of determining damping follows:

a. Half-Power Bandwidth: While probably not appropriate for high damping devices such as the isolators of interest in this work, the technique involves determining $\Delta\omega$ and ω_{res} where $\Delta\omega$ is the bandwidth $\omega_2-\omega_1$, between two amplitudes usually taken as 0.707 A_{max}. A_{max} is the response peak at ω_{res}. For viscous damping, this results in:

$$\frac{\Delta\omega}{\omega_{res}} = 2\zeta \tag{2.1}$$

while for hysteretic damping:

$$\frac{\Delta\omega}{\omega_{res}} = \sqrt{1+\eta} - \sqrt{1-\eta} \tag{2.2}$$

Note that the right-hand side of Eq. (2.2) equals η for $\eta<<1$.

b. Resonant Response Amplitude: In this method, an amplitude A is defined, Eq. (2.3), and determined experimentally.

$$A = \frac{(W_p)_{res}}{F/k} = \frac{\text{amplitude of response at resonance}}{\text{static displacement}} \tag{2.3}$$

For viscous damping, Eq. (2.3) becomes

$$A = \frac{1}{2\zeta\sqrt{1-\zeta^2}} = \frac{1}{2\zeta} \text{ for } \zeta<<1 \tag{2.4}$$

while for hysteretic damping:

$$A = \frac{1+\eta^2}{\eta} = \frac{1}{\eta} \text{ for } \eta<<1 \tag{2.5}$$

c. Use of a Nyquist Diagram which is equivalent to a, above.

d. Hysteresis Loops: The area contained within a force versus deflection plot over one cycle of motion equals the energy dissipated per cycle, D_s. The simplest example of this is that of base excitation of a single degree of freedom system which can be shown to yield, for viscous damping:

$$D_s = \pi\, c\, \omega\, W_r^2 \tag{2.6}$$

and for hysteretic damping:

$$D_s = \pi\, k\, \eta\, W_r^2 \tag{2.7}$$

In Eqs. (2.6) and (2.7), W_r is the relative displacement between the single mass and the base, ω is the forcing frequency, while c, k, and η are the properties of the viscous, c, and hysteretic, $k(1+i\eta)$, dampers.

Expressions which are alternatives to Eqs. (2.6) and (2.7) are derived by Nashif, et al., and are

$$D_s = \frac{\pi\, \eta\, k\, \xi^4\, W_o^2}{(1-\xi^2)^2 + \eta^2} \tag{2.6a}$$

and

$$D_s = \frac{\pi c \omega \xi^4 W_o^2}{(1-\xi^2)^2 + (c\omega/k)^2} \tag{2.7a}$$

In Eqs. (2.6a) and (2.7a), two new terms appear. They are:

$$\xi^2 = \frac{m\omega^2}{k}$$

W_o = amplitude of harmonic steady state base motion

While this technique seems to hold the greatest promise for application to the isolators of interest, it should be noted that all equations (2.6-7a) are for single degree of freedom models with constant properties.

e. Quadrature Bandwidth: In this method, the imaginary part of the response, α_Q is plotted versus frequency and two points on opposite sides of the peak are located by $\frac{1}{n}\alpha_Q$. The $\Delta\omega_Q$ between these points is then found. For $n = \sqrt{2}$, the relationship can be shown to be:

$$\frac{\Delta\omega_Q}{\omega_{res}} = \sqrt{1 + 0.6436\eta} - \sqrt{1 - 0.6436\eta} \tag{2.8}$$

If $\eta \ll 1$, then using the binomial theorem, Eq. (2.8) becomes

$$\frac{\Delta\omega_Q}{\omega_{res}} = (1 + 0.3218\eta) - (1 - 0.3218\eta) + \ldots \simeq 0.6436\eta \tag{2.9}$$

Hence,

$$\eta \simeq 1.554 \frac{\Delta\omega_Q}{\omega_{res}} \tag{2.10}$$

f. Dynamic Stiffness: For a single degree of freedom hysteretic model, the complex ratio of displacement excitation gives the form:[1]

---

[1]Craig, R. R., Structural Dynamics, Wiley, 1981, p. 101.

$$\alpha = \frac{W_p^*}{F} = \frac{1}{k - m\omega^2 + ik\eta} \tag{2.11}$$

which can also be written in the form

$$\alpha = |\alpha|e^{i\phi} = \alpha_D + i\alpha_Q \tag{2.12}$$

If $|\alpha|$ and ϕ are measured experimentally, Nashif, et al., note the difficulty (though not impossible) of determining k and η by solving the four equations for $|\alpha|$, ϕ, α_D, and α_Q.[2] Alternatively, one may define the dynamic stiffness as $K = 1/\alpha$. Therefore

$$K = k - m\omega^2 + ik\eta = K_D + iK_Q \tag{2.13}$$

where K_D is called the direct dynamic stiffness and

K_Q is the quadrature dynamic stiffness.

Equating real and imaginary parts of Eq. (2.13) yields

$$K_D = k - m\omega^2 = \frac{\cos\phi}{|\alpha|} \tag{2.14}$$

$$K_Q = k\eta = \frac{\sin\phi}{|\alpha|} \tag{2.15}$$

Plotting $K_D + m\omega^2$ versus frequency and $K_Q/(K_D + m\omega^2)$ versus frequency yields

$$k = K_D + m\omega^2 \tag{2.16}$$

$$\eta = \frac{K_Q}{K_D + m\omega^2} \tag{2.17}$$

Nashif, et al., note that this method is very helpful when η is high.

Turning from single degree of freedom considerations, techniques for damping analysis vary widely. The authors contend that ultimately

---

[2]Nashif, et al., Vibration Damping, Wiley, 1985, pp 142, 145.

the use of finite element software probably holds the best promise for solving very complicated geometric arrangements of wire rope. Nashif, et al., discuss the merits and pitfalls of such an approach. Treatment of damping phenomena by this method is far from trivial, however, and greater insight into the basic mechanisms has been the intent of this study.

Attempts to date using finite element techniques for this research period are discussed in Sections 4 and 5.

3. STATIC MODELS

Background

The uses of stranded cables in conventional engineering applications are well recognized. For rope-selection and handling, practicing engineers have long depended upon extensive experimental results, such as those compiled by Scoble (1920-1928) that began to appear in the early 1900s. More recently, the Wire Rope Board and federal agencies (1980) have utilized the available empirical data to provide general guidelines for rope selection. Attempts to correlate the experimental data have met with some success (Druckers and Tachau, 1945; Huang, 1975), yet these fall short of an in-depth understanding of the effects of various wire-rope parameters on their static and dynamic behavior. In view of the recently proposed applications of wire ropes for augmentation of structural damping in large space structures, the importance of such theoretical static and dynamic investigations has increased considerably.

Of the various investigations, special significance is attached to the work of Costello and Phillips (1973, 1974) who adopted a more basic approach to study the static behavior of the cables. Here the cables were treated as groups of separate curved rods (Love, 1944) in the form of helices. This static analysis leads to a set of nonlinear algebraic equations in several variables. These equations are solved simultaneously using the Newton-Raphson algorithm. However, the utility of the analysis is severely limited as it depends on computational

results obtained for particular cases of cable data. For design, it would be far more desirable to have the solution in analytical form that can provide an insight into the influence of the various wire rope parameters on its deformation characteristics. Such analytical results may be of even greater significance for the future investigations of wire rope dynamics.

Summary

To obtain the analytical solutions, we separately consider two different models of cables (Fig. 3.1). In the first, the cable is assumed to be a single strand constituted by a single layer of an arbitrary number of thin helical wires. The core is assumed to be fibrous so that it does not contribute to the strength of the rope directly. In the second model, the cable has a metallic wire core that is wrapped around by an arbitrary number of layers of helical wires, each having its own direction and magnitude of lay. In either of the two cases, we assume that an axial force, F, and an axial or torsional moment, M, when applied to the cable cause it to undergo elongation as well as "twist." This results in elongation, changes in the lay angles and helix radii of helical wires in each of the layers. An assumption of small changes in the wire helix angle and helix radius is utilized to develop simple governing linear relations for the applied forces and moments in terms of the linear and rotational cable strains.

A summary of static analyses follows:

a. Cables with Fibrous Cores.

The results characterizing the deformation characteristics can be summarized as follows:

(i) The longitudinal strain, ξ, in the helical wire and the overall cable strain, ε, are related by

$$\xi = \varepsilon - \Delta\alpha \cot \alpha \, . \tag{3.1}$$

where

α = lay angle of helical wires when cable is not loaded

$\Delta\alpha$ = increment in helix angle due to the applied load

(ii) The expression for rotational strain, β, is given by

$$\beta = (1+\nu)\, \varepsilon \cot \alpha - (\Delta\alpha/\sin^2\alpha)[1 - (f-\nu) \cos^2\alpha] \tag{3.2}$$

where

ν = Poisson's ratio of wire material

$$f = [1 - \sin^2\alpha \sin^2(\pi/m)\{1+\sin^2(\pi/m)\cos^2\alpha\}]$$

(iii) The effective Modulus of Rigidity has been obtained for two different end conditions:

$\beta = 0$: When the free cable end is not permitted to rotate under end moment constraints, i.e., when $\beta=0$, the expression for the effective modulus of rigidity can be written as

$$(\bar{E})_{\beta=0} = g \sin \alpha \tag{3.3}$$

where $\bar{E} = \dfrac{F}{AE\varepsilon}$

A = metallic area of the cross-section

E = modulus of rigidity of the wire material

$$g = [1 - (1+\nu)\cos^2\alpha - (1+\nu)\{\cos^2(\pi/m) - \nu\} \cos^4\alpha]$$

M = 0: When the axial (torsional) moment M=0, the expression for the modulus of rigidity, $\bar{E}$, takes the form:

$$(\bar{E})_{M=0} = (\bar{E})_{\beta=0}\ 1-[1-\{\sin^4\alpha\ \sin^2(\pi/m)((1+\nu)\cos^2\alpha + (1+\nu_f\ \cos\ 2\alpha))\}/$$
$$\{4h\ \cos^2\alpha + \sin^4\alpha\ \sin^2(\pi/m)((1+\nu)\sin^2\alpha\ \cos^2\alpha$$
$$+(1+\nu_f\cos 2\alpha))\}][1-\{(1/4)\sin^2\alpha\ \sin^2(\pi/m)$$
$$\{(1+\nu\ \sin^2 2\alpha)/(1+\nu)\}/g] \qquad (3.4)$$

where

$$h = [1+\{\cos^2(\pi/m)-\nu\}\cos\alpha^2 + (1-2\nu)\cos^4\alpha]$$

Figure 3.2 shows a comparison of the values of effective modulus of rigidity for cables obtained using the above analytical results with the corresponding numerical results of Costello and Phillips (1976) over the entire feasible range of α. A generally excellent agreement between the two is noted, thus establishing the validity of the approximate analytical approach adopted here.

b. Cables with metallic core

The above approximate analytical approach is now applied to investigate the various deformation characteristics in a more general cable model. Here, we consider that the core wire is metallic and large enough to prevent helical wires in a layer from touching each other, although these wires remain in contact with those in the adjacent layers. We assume the cable to be made up of n successive layers, counting from the innermost core which is taken as the first layer. The results characterizing the deformation properties of such a cable are summarized below:

(i) The longitudinal strain in helical wires in the ith layer denoted by ξ_i and the overall longitudinal cable strain, ε, are related by

$$\xi_i = \varepsilon - \Delta\ \alpha_i \cot \alpha_i \quad , \quad i = 1,2,3,\ldots,n \tag{3.5}$$

where

α_i = original lay angle of the helical wires in the ith layer.

$\Delta\alpha_i$ = increment in the lay angle of the helical wires in the ith layer when load is applied.

(ii) The expression for $\Delta\alpha_i$ can be written as

$$\Delta\alpha_i = \varepsilon(1+\nu)(1-\nu_i)\sin \alpha_i \cos \alpha_i[1 - 2 \sum_{j=2}^{i-1} \{(r_j/r_i)\nu_j\}]$$

$$-\beta(r_i/R)(1-\nu_i)\sin^2 \alpha_i[1 - 2 \cot \alpha_i \sum_{j=2}^{i-1} \{\nu_j(r_j/r_i)^2 \tan \alpha_j\}] \tag{3.6}$$

where

r_j = helix radius of the helical wires in the jth layer;

$j = 1,2,\ldots, i,\ldots,n.$

R_j = radius of the helical wires in the jth layer;

$j = 1,2,\ldots, i,\ldots,n.$

$\nu_j = \nu(R_j/r_j) \cos^2\alpha_j$; $\quad j=1,2,\ldots, i, \ldots n.$

R = radius of the cable.

(iii) The expressions for the applied force, F, and applied moment, M, can be stated in the following convenient linear form:

$$\bar{F} = F_\varepsilon\ \varepsilon + F_\beta\ \beta \tag{3.7}$$

$$\bar{M} = M_\varepsilon\ \varepsilon + M_\beta\ \beta \tag{3.8}$$

where

$\bar{F} = F/(AE)$

$\bar{M} = M/(ER^3)$

A = metallic area of cross-section; $\sum_i (m_i R_i^2)$

E = modulus of rigidity of the cable material

R = cable-radius

m_i = number of helical wires in the ith layer

R_i = radius of the helical wires in the ith layer

$\bar{R}_i = R_i/R$

$$F_\varepsilon = \sum_i [m_i R_i^2 \sin\alpha_i(\sin\alpha_i - \nu\cos^2\alpha_i)] / \sum_i [m_i R_i^2]$$

$$F_\beta = \sum_i [m_i R_i^2 (r_i/R)\sin^2\alpha_i \cos\alpha_i] / \sum_i [m_i R_i^2]$$

$$M_\varepsilon = \pi \sum_i [m_i \bar{R}_i^3 \cos\alpha_i \{(r_i/R_i)(\sin^2\alpha_i - \nu\cos^2\alpha_i) - (1/4)(R_i/r_i)\}]$$

$$M_\beta = \pi \sum_i [m_i \bar{R}_i^4 \sin\alpha_i \{(r_i/R_i)^2 \cos^2\alpha_i + (1/4)(1+\nu_f \sin^4\alpha_i \cos 2\alpha_i)\}]$$

Next, we demonstrate the usefulness of the analytical results by applying these to study some important extensional and torsional stiffness characteristics of wire ropes.

Effective Modulus of Rigidity ($\bar{E}$)

(a) No end rotation; i.e., $\beta=0$: Here the expression for the effective modulus of rigidity can be written as

$$(\bar{E})_{\beta=0} = F_{\varepsilon} = \sum_i [m_i R_i^2 \sin \alpha_i (\sin^2 \alpha_i - \nu \cos^2 \alpha_i)] / \sum_i [m_i R_i^2] \qquad (3.9)$$

(b) Cable ends free to rotate; i.e., M=0: Here, we obtain

$$\begin{aligned}(\bar{E})_{M=0} = {} & \sum_i [m_i R_i^2 \sin \alpha_i (\sin^2 \alpha_i - \nu \cos^2 \alpha_i)] / \sum_i (m_i R_i^2] \\ & - \sum_i [m_i \bar{R}_i^2 (r_i/R) \sin^2 \alpha_i \cos \alpha_i] \sum_i [m_i \bar{R}_i^3 \cos \alpha_i \\ & \{(r_i/R_i)(\sin^2 \alpha_i - \nu \cos^2 \alpha_i) - (1/4)(R_i/r_i)\}] / [\sum_i [m_i \bar{R}_i^2] \cdot \\ & \sum_i [m_i \bar{R}_i^4 \sin \alpha_i \{(r_i/R_i)^2 \cos^2 \alpha_i \\ & + (1/4)(1+\nu_f \sin^4 \alpha_i \cos 2\alpha_i)\}]] \ . \end{aligned} \qquad (3.10)$$

Effective Torsional Modulus of Rigidity ($\bar{G}$)

Effective torsional modulus of Rigidity ($\bar{G}$) is given by

$$\bar{G} = \pi[\sum_i m_i \bar{R}_i^4 \sin \alpha_i \{(r_i/R_i)^2 \cos^2 \alpha_i + (1/4)(1+\nu_f \sin^4 \alpha_i \cos 2\alpha_i)\}$$

$$- \sum_i [m_i \bar{R}_i^3 \cos \alpha_i \{(r_i/R_i)(\sin^2 \alpha_i - \nu \cos^2 \alpha_i)$$

$$- (1/4)(R_i/r_i)\}] \cdot$$

$$\sum_i [M_i \bar{R}_i^3 (r_i/R_i) \sin^2 \alpha_i \cos \alpha_i] / \sum_i [m_i \bar{R}_i^2 \sin \alpha_i (\sin^2 \alpha_i$$

$$- \nu \cos^2 \alpha_i)]] \qquad (3.11)$$

To illustrate the ease of application, we consider a specific cable with the following data:

- First layer (or metallic core):

  $m_1 = 1, \quad \alpha_1 = \pi/2, \quad R_1 = a$

- Second layer:

  $m_2 = 6, \quad \alpha_2 = \alpha, \quad R_2 = a$

- Third layer:

  $m_3 = 12, \quad \alpha_3 = \pi - \alpha, \quad R_3 = a$

Evidently, the above three characteristics, $(\bar{E})_{\beta=0}$, $(\bar{E})_{M=0}$, and $\bar{G}$, would be dependent on the value of α chosen. Figure 3.3 shows the effect of varying this lay angle α on the stiffness properties of the cable. In all cases, effective extensional modulus of rigidity significantly decreases as α decreases. The stiffness remains higher, however, for the case of "fixed ends" when the rotational strain is zero.

Figure 3.4 presents the effect of varying α on the torsional stiffness. Here the trend is reversed as increasing α leads to rapid fall in the torsional rigidity of the cables. Needless to say, such plots could be readily generated for any arbitrary situation, thus facilitating the choice of geometric parameters of the cable.

Application to Dynamic Investigations

To illustrate the usefulness of the analytical results in dynamic studies, consider a vertically hanging cable clamped at the upper end and carrying a weight at its free end. The differential equations governing the cable "extension-twist" oscillations (assuming the weight of the cable itself to be negligible) can be written as

$$(d^2\varepsilon/dt^2) = -\frac{AE\ g}{W\ell}\ [F_\varepsilon\ \varepsilon + F_\beta\ \beta] \tag{3.12}$$

$$(d^2\beta/dt^2) = -\frac{R^4 Eg}{I\ell}\ [M_\varepsilon\ \varepsilon + M_\beta\ \beta] \tag{3.13}$$

where

W = weight of the hanging mass

I = moment of inertia of the mass (related to cable twist)

ℓ = length of the cable

It is now easy to determine the frequency of the coupled oscillations. The expression for the natural frequencies (ω) of the coupled oscillations can be written as

$$\omega^2 = (1/2)(Eg/\ell)[AF_\varepsilon/W) + (R^4\ M_\beta/I) \pm\{(AF_\varepsilon/W - R^4 M_\beta/I)^2 + 4\ AR^4\ F_\beta M_\varepsilon/(WI)\}^{1/2}] \tag{3.14}$$

The dimensionless analytical force and torsional moment relations developed here are rather general. The explicit form of results is found to be useful in predicting the rope stiffness against elongation as well as rotation. The examples considered here demonstrate the computational ease and effectiveness with which the closed-form solution can be utilized in various studies. The results of the static analyses would be quite useful in dealing with any general problem of wire rope dynamics. Finally, the valuable insight thus gained into the relative deformation behavior of wire strands is likely to facilitate modeling of energy dissipation in the rope through internal rubbing action.

4. SIMPLEST DYNAMIC MODELS

One-Dimensional Models

It is possible to postulate several spring-mass-damper one-dimensional isolator models. These models include an undamped model, a rigidly connected Coulomb damper model, and an elastically connected Coulomb damper model. In Fig. 4.1 is shown the wire rope vibrator isolator being modeled, and in Figs. 4.2 through 4.4 are shown the simplest mathematical models studied.

For the isolator shown in Fig. 4.1, an experimental study has been performed to determine the frequency response characteristics. The experimental arrangement consisted of exciting the base vertically. Most of the isolator frequency response data is presented in Appendix A.

In Table I are shown the numerical values of acceleration and displacement for the isolator base and center mass shaker test. A plot of this experimental data appears with analytical curves discussed and referred to below.

For use in an analytical comparison, an experimental stiffness curve has been obtained. The arrangement used for the stiffness measurements was as follows. The isolator was mounted vertically; upside-down from the position shown in Fig. 4.1. A horizontal metal strip was attached to the center mass of the isolator with an LVDT arranged at its opposite end to measure mass displacement. The procedure used in the measurements was to apply known static loads to the isolator center mass and monitor the downward displacement by use of

the LVDT and a voltmeter. The stiffness curve is shown in Fig. 4.5 and is seen to be nonlinear. The average stiffness is approximately 100 lb/in.

The governing equation of motion for the model shown in Fig. 4.2 is

$$M\ddot{x} + K(x-u) = 0 \tag{4.1}$$

where x and u are positive as shown in the figure and M and K are the mass and stiffness, respectively. The weight of the center mass for the isolator is 0.1359 lb, and the stiffness used (an average value) is 97.656 lb/in. Equation (4.1) was solved using the Advanced Continuous Simulation Language (ACSL) in preparation for more involved model solutions. A listing of the program is shown in Fig. 4.6. In Fig. 4.7 is shown a comparison of the frequency response for the experimental arrangement, previously described, and the undamped model of Fig. 4.2 as solved by ACSL. The mass displacement for the undamped model is higher than the mass displacement for the real isolator at all frequencies as was expected. However, Fig. 4.7 does show that the undamped one-dimensional model displays the same basic behavior as that of the real isolator. Of course, the response of the undamped model increases without bound at the natural frequency of the model. The natural frequency of the undamped model is approximately 84 Hz, while the resonant frequency of the real isolator is approximately 75 Hz. Figure 4.7 is significant because it shows that one-dimensional models hold promise for modeling the behavior of, at least, the uni-axial motion of the isolator. From these results, it would be expected that by incorporating damping into the model, good results would be obtained. This was the next step taken in the analytical study.

It has been surmized that the damping in wire rope isolator systems is dry friction, or Coulomb, damping. By incorporating a friction force in the equation of motion, a mathematical model of the system shown in Fig. 4.3 is obtained. The equation of motion is

$$M\ddot{x} + K(x-u) + \text{sgn}(\dot{x})\, F_f = 0 \qquad (4.2)$$

where F_f is the Coulomb friction force which always opposes the motion of the mass. As a first approximation, it was assumed that the friction force is constant for all frequencies. Using a constant force of 2.25 lb, the mass displacement response shown in Fig. 4.8 was obtained, again using ACSL. It is seen that the model is overdamped for most of the frequency range. These results led to the investigation of frequency dependence of the friction force F_f. It was found that for low frequencies (below 60 H_z) the analytical mass response is not as sensitive to changes in the friction force F_f as it is at higher frequencies. Using the values of F_f shown in Table II, the frequency response shown in Fig. 4.9 was obtained. It is seen that this model is in much better agreement with experiment than the model which assumes no frequency dependence of the friction force. It is interesting to note that for the Coulomb-damped models, the natural frequency is about 80 Hz, slightly lower than the resonant frequency of the undamped model.

The insensitivity of the Coulomb-damped model to changes in F_f at low frequencies suggests that the isolator might best be modeled as an elastically connected Coulomb damper system as shown in Fig. 4.4.

To date, good results as described above have been obtained for the displacement response of the Eq. (4.2) model. An analytical hysteresis loop, generated by the ACSL model with variable friction force, is shown in Figure 4.10. The acceleration response of the mathematical model, however, has not agreed well with experiment. This needs further study.

NASTRAN Single Loop Model

A NASTRAN bar element model in the form of an ellipse has been generated. Table III is a program listing. There are 100 grid points symmetrically arranged to match geometrically the single wire rope loop test to be described. Those grid points in the region of the clamped portion of the ellipse are fixed against any movement; those in the region of the sliding block (to be described) are allowed only translation in the direction perpendicular to the plane of the loop. All other grid points are allowed six degrees of freedom. A restricted parameter study has been carried out with the following as parameters: E, G, A, I_x, I_y, and J. Appendix B summarizes the computation of several of these.

A tentative conclusion at this point is that varying E and G can result in a stiffness value equal to that obtained experimentally; however, questions still remain concerning the validity of the parameter values used. In general, E and G values seem to have to be lowered an order of magnitude more than those reasonably expected in order to agree with experiment. This geometric (looped) case has not yet been solved analytically like the other simpler cases in SECTION 3, however.

Single-Loop Wire Rope Tests

A single wire rope loop has been mounted in a special device which has the capability to clamp one "side" of the elliptical loop. The opposite "side," though free to move perpendicularly to the plane of the wire rope loop, prevents the wire rope from experiencing any degrees of freedom other than this one. In this manner, one "loop" of a typical wire rope isolator is simulated. The means by which such a restrictive motion is accomplished is through the use of two low friction linear bearings which fit closely on a close tolerance shaft. The block which houses the bearings also has the means to clamp the moving "side" of the wire rope loop. Figure 4.11 is a photograph of this particular test arrangement. Interestingly, if only one half of the wire rope loop is attached, the bearings and their housing "roll" about the shaft as the loop is moved perpendicular to its plane. No such "roll" is observed with a symmetrical loop in place.

No attempt was made to match the size of wire rope tested in the aforementioned device with the actual size used for the candidate isolator. This is primarily due to the impractical small bearing/shaft dimensions required to do so. Instead, it was decided that a larger loop would exhibit a phenomenon similar to a smaller loop and our research would center on exploration of such at present.

To date, tests have been performed primarily to ascertain wire rope stiffness values for comparison with the NASTRAN model already described. The arrangement should be more significant when the static models in Section 3 are extended to the combined bending/twisting case,

and/or the bending/twisting/extension case which should more realistically describe the isolator application.

Another test being planned is a dynamic test to determine the hysteresis loop for a single wire rope loop. It is very likely that this will have to involve two loops (both in the same plane, symmetrically arranged to each side of the bearing/shaft movement) and a special two-point shaker excitation scheme with at least two dynamic force gages.

Using traditional terminology of a 2a x 2b elliptical loop of wire rope, loops with large values of a/b are less stiff than those with a/b values approaching unity. The table below gives specific experimental values:

a/b	2a (inches)	2b (inches)	Lgth of Cable (inches)	Stiffness (lbs/in.)
1.11	2.5	2.25	7.461	5.138
1.22	2.75	2.25	7.854	3.292
1.44	3.25	2.25	8.639	2.144

Experimental force versus deflection curves, while not shown, are reasonably linear.

Isolator-Supported Momentum Wheel Equations

Consider a momentum wheel of mass M supported by three symmetrically spaced uniaxial isolators. The momentum wheel, while symmetrical, has an unbalanced mass m offset by a distance e from its spin axis. Figure 4.12 shows both a side view and a top view of the disc, axes, etc. For the spin axis z, and an imaginary fixed plane which contains m and e located by the coordinate ϕ from x, the modified Euler equations are (Meriam, 1975):

$$\Sigma M_x = I_{xx}\dot{\Omega}_x - (I_{yy}-I_{zz})\Omega_y\Omega_z + I_{zz}\dot{\phi}\Omega_y$$

$$\Sigma M_y = I_{yy}\dot{\Omega}_y - (I_{zz}-I_{xx})\Omega_z\Omega_x - I_{zz}\dot{\phi}\Omega_x \qquad (4.3)$$

$$\Sigma M_z = I_{zz}\dot{\Omega}_z + I_{zz}\ddot{\phi}$$

Using Fig. 4.12 and assuming that the eccentric mass m is a distance h above point 0, the left-hand sides of Eqs. (4.3) can be found to be

$$\Sigma M_x = -mg\ e\ \sin\phi + R_1 R\cos\alpha_1 - R_o\ R\ \cos\alpha_2 + R_2 R\ \sin\alpha_3$$
$$+ me(\dot{\Omega}_z + \ddot{\phi})h\ \cos\phi - me(\Omega_z{}^2 + \dot{\phi}^2)h\ \sin\phi$$

$$\Sigma M_y = mge\ \cos\phi - R_1 R\ \sin\alpha_1 + R_2 R\ \cos\alpha_3 - R_o R\ \sin\alpha_2 \qquad (4.4)$$
$$+ me(\Omega_z{}^2 + \dot{\phi}^2)h\ \cos\phi + me(\dot{\Omega}_z + \ddot{\phi})h\ \sin\phi$$

$$\Sigma M_z = -me^2(\dot{\Omega}_z + \ddot{\phi}) + M_z(t) - 3RR_t$$

where $\alpha_1 = \Omega t + \pi/2 - 120° = \Omega t + \frac{3}{6}\pi - \frac{4}{6}\pi = \Omega_z t - \frac{\pi}{6}$

$$\alpha_2 = 2\pi - \frac{3}{2}\pi - \Omega t = \frac{\pi}{2} - \Omega_z t$$

$$\alpha_3 = \Omega t + \pi - 2\left(\frac{2}{3}\pi\right) = \Omega_z t - \frac{\pi}{3}$$

and R_t = tangential reactions at each isolator pair.

The simplest form of the support forces would be in the form of k times deflection. These are

$$R_1 = k_1(R\theta_x \cos \alpha_1 - R\theta_y \sin \alpha_1)$$

$$R_2 = k_2(R\theta_x \sin \alpha_3 + R\theta_y \cos \theta_3) \qquad (4.5)$$

$$R_o = - k_o(R\theta_x \cos \alpha_2 + R\theta_y \sin \alpha_2)$$

$$R_t = k_t R\phi$$

Actually the k's shown in Eq. (4.5) will be modified to reflect a more realistic Coulomb friction support action.

The mass moment of inertia of the disc referred to point 0, ignoring the eccentric mass m (m<<M), is

$$[I]_o = \begin{bmatrix} \frac{1}{4} MR^2 + \frac{1}{3} M(2h)^2 & 0 & 0 \\ 0 & \frac{1}{4} MR^2 + \frac{1}{3} M(2h)^2 & 0 \\ 0 & 0 & \frac{1}{2} MR^2 \end{bmatrix} \qquad (4.6)$$

Also needed are the relationships between the θ's and Ω's which are

$$\theta_x = \int \Omega_x dt \qquad \theta_x(0) = 0°$$

$$\theta_y = \int \Omega_y dt \qquad \theta_y(0) = 0° \qquad (4.7)$$

$$\theta_z = \int \Omega_z dt \qquad \theta_z(0) = 0°$$

The set of equations ((4.3) through (4.7)) can be solved for the highest ordered derivatives and integrated numerically. A scheme to do this with ACSL is shown in Fig. 4.13 with the additional capability of incorporating the successful model-with-variable-friction-force into the

simulation as a multiply-invoked MACRO. Vector integrators can be conveniently used to handle the θ and Ω relationships. Vector operations are shown in Fig. 4.13 by the { } brackets. A parameter which would be a measure of successful isolation is postulated as

$$\theta_{max} = \sqrt{\theta_x^2 + \theta_y^2 + \phi^2} \tag{4.8}$$

θ_{max} equals zero would be perfect isolation. It should be noted that the three variables in Eq. (4.8) vary with time, in general, so that peak-to-peak or rms values would be most meaningful for the general case. Actual parametric runs on the computer exceed the scope of this phase of the research. An anticipated form of the output is shown in Fig. 4.14.

5. ADVANCED DYNAMIC MODELS

Basic Finite Element Models

For the purpose of preliminary analysis, three NASTRAN finite element models have been developed. Two of these are complete models (i.e., including all seven strands--six wound and one maiden) of a line segment of the cable. The other is an incomplete model of the same line segment, which has been developed as a geometric check for the complete models.

The incomplete model, hereafter referred to as "the two strand model," was the first to have been developed. This model consists of a maiden strand around which a single strand is wound (see Fig. 5.1). Both the maiden and the wound strands are subdivided into 276 elements; each strand requiring 1932 grid points for definition. The hexagonal cross section of each strand consists of six triangular segments (see Fig. 5.2). Each triangular segment represents the upper (or lower) surface of solid "pie-shaped" PENTA elements (solid triangular elements used in MSC-NASTRAN). Figure 5.3 shows a typical PENTA element. The thickness of each element (0.002 inches) is twice the length of each element. This results in the maiden strand being 0.09 inches in length and 0.002 inches in diameter. That is, the line segment modeled has a L/D ratio of 45.

The wound strand forms a helix angle of 72 degrees. Both strands are connected by scalar elastic elements (springs), which were incorporated to model the normal forces acting on each strand. Figure 5.2 shows the arrangement of the scalar elastic elements.

The complete models are similar to the two strand model with one exception; that is, the complete models consist of a maiden strand and six wound strands. Hence, the name, "seven strand model." The wound strands are connected to the maiden strand and to adjoining wound strands by springs. A typical cross section of a seven strand model is shown in Fig. 5.4. Also shown in this figure is the arrangement of the spring elements.

The difference in the two seven-strand models occurs in their boundary conditions. Both models are suspended at one end. The first model has the other end free, thus forming a fixed-free line segment of the wire rope (see Fig. 5.5). The second model has a mass attached to the other end of the wire rope (see Fig. 5.6). This model has been designated as simply "the pendulum model". The tip mass, M, is one and one-half times as heavy as the wire rope.

Equations of Motion

The deformation of the cable was modeled using the assumed modes method. Using this method, the position vector of a generic mass element (see Fig. 5.7), dm, can be expressed as

$$\underline{r}_{dm} = \sum_{j=1}^{m} \underline{\phi}_j \, q_j \tag{5.1}$$

where $\underline{\phi}_j$ are the mode shape vectors, and q_j are the generalized coordinates. The mode shape vectors, $\underline{\phi}_j$, are functions of the undeformed coordinates, x_o, y_o, and z_o. They were obtained from the MSC NASTRAN finite element models described above.

The equations of motion were obtained via a Lagrangian approach. To formulate the Lagrangian, the potential and kinetic energies of the wire rope segment are required. The former is the sum of the elastic and gravitational potential energies. For the contribution due to the elasticity of the system, we can write

$$V_s = 1/2\ \underline{q}^T\ \underline{\underline{K}}_s \underline{q} \tag{5.2}$$

where $\underline{\underline{K}}_s$ is the system's stiffness matrix and $\underline{q} = (q_1\ q_2 \cdots q_n)^T$.

The following assumptions were made in order to formulate the gravitational potential energy:

i. length of segment = L

ii. mass per unit length = σ

iii. small displacements in the xz-plane

With these assumptions, the expression for the gravitational potential energy becomes

$$V_g = 1/2\ \underline{q}^T\ \underline{\underline{K}}_g\ \underline{q} \tag{5.3}$$

where $\underline{\underline{K}}_g$ is the gravitation stiffness matrix. The matrix, $\underline{\underline{K}}_g$ is given by

$$\underline{\underline{K}}_g = 1/2 \sum_{i=0}^{N-1} \int_0^L \sigma_i \int_0^{z_o} [\underline{\underline{\Phi}}']^T [\underline{\underline{\Phi}}']\, d\xi\ dz_o \tag{5.4}$$

where $\underline{\underline{\Phi}}' = (100)\frac{d}{dz}(\Phi)$ and $\underline{\underline{\Phi}} = (\underline{\Phi}_1\ \underline{\Phi}_2 \cdots \underline{\Phi}_m)$. In the case of the pendulum model, the gravitational stiffness matrix also has the following term added to it:

$$1/2\ M \int_0^L [\underline{\Phi}']^T[\underline{\Phi}']\ dz_o$$

With the cable fixed at the upper end, the kinetic energy of the pendulum system can be expressed as

$$T = 1/2 \sum_{i=0}^{N-1} \int_{m_i} \dot{\underline{r}}_{dm}^T \dot{\underline{r}}_{dm}\ dm + 1/2\ M\ \dot{\underline{r}}_m^T \dot{\underline{r}}_m \tag{5.5}$$

where $\dot{\underline{r}}_{dm}$ and $\dot{\underline{r}}_m$ are the velocities of a generic mass element, and the tip mass, respectively. N represents the number of strands included in the model. The strands are numbered such that the maiden strand is i=0, and the others are numbered in a counterclockwise manner beginning with i=1. Using Eq. (5.1), the expression for the kinetic energy can be rewritten as

$$T = 1/2\ \dot{\underline{q}}^T\ \underline{\underline{M}}\ \dot{\underline{q}} \tag{5.6}$$

where $\underline{\underline{M}}$ is the generalized mass matrix given by

$$\underline{\underline{M}} = \sum_{i=1}^{N-1} \int_{m_i} \underline{\underline{\Phi}}^T \underline{\underline{\Phi}}\ dm + M[\underline{\underline{\Phi}}]^T[\underline{\underline{\Phi}}] \tag{5.7}$$

where the bracketed Φ terms are evaluated at the lower end. For the seven-strand model without the weight, the second term in Eq. (5.7) is neglected (i.e., M=0).

The nonconservative forces acting on dm are assumed to be due to viscosity and Coulomb friction between the strands. Generalized viscous damping forces are modeled as

$$\underline{Q}_v = - \left[\underline{\underline{D}}\right] \dot{\underline{q}} \tag{5.8}$$

where $[\underline{\underline{D}}]$ is a diagonal matrix of structural damping coefficients. The generalized Coulomb damping forces are obtained from

$$Q_c = \sum_{i=0}^{N-1} \int_{m_i} \underline{\underline{\Phi}}^T \underline{f}_{dm_i} dm \tag{5.9}$$

where $\underline{f}_{dm_i}$ denotes the force on an element dm of the i^{th} strand. If μ denotes the coefficient of friction between the strands, and f_{ij} denotes the magnitude of the normal force between the i^{th} and j^{th} strands, then for the maiden strand, $\underline{f}_{dm_o}$ becomes

$$\underline{f}_{dm_o} = \sum_{i=1}^{N-1} \mu f_{oi} \operatorname{sgn}[(\dot{\underline{r}}_{dm_o} - \dot{\underline{r}}_{dm_i}) (\hat{\underline{t}}_i \hat{\underline{t}}_i + \hat{\underline{b}}_i \hat{\underline{b}}_i) \tag{5.10}$$

$\hat{\underline{t}}_i$ and $\hat{\underline{b}}_i$ are the unit tangent and binormal vectors, respectively, of dm_i. For the other strands, we have

$$\begin{aligned} \underline{f}_{dm_i} = \mu \{ & f_{oi} \operatorname{sgn}[(\dot{\underline{r}}_{dm_o} - \dot{\underline{r}}_{dm_i}) \cdot (\hat{\underline{t}}_i \hat{\underline{t}}_i + \hat{\underline{b}}_i \hat{\underline{b}}_i)] \\ & - f_{ij} \operatorname{sgn}[(\dot{\underline{r}}_{dm_i} - \dot{\underline{r}}_{dm_j}) \cdot (\hat{\underline{t}}_i \hat{\underline{t}}_i + \hat{\underline{b}}_i \hat{\underline{b}}_i)] \\ & - f_{ik} \operatorname{sgn}[(\dot{\underline{r}}_{dm_i} - \dot{\underline{r}}_{dm_k}) \cdot (\hat{\underline{t}}_i \hat{\underline{t}}_i + \hat{\underline{b}}_i \hat{\underline{b}}_i)] \} \end{aligned} \tag{5.11}$$

with

$$\begin{bmatrix} i \\ j \\ k \end{bmatrix} = \begin{bmatrix} 1 \\ 2 \\ 6 \end{bmatrix}, \begin{bmatrix} 2 \\ 3 \\ 1 \end{bmatrix}, \begin{bmatrix} 3 \\ 4 \\ 2 \end{bmatrix}, \ldots \tag{5.12}$$

The unit tangent and binormal vector are given by

$$\hat{\underline{t}}_i = \cos\ \alpha[-\sin\ \theta_i\ \hat{\underline{i}} + \cos\ \theta_i\ \hat{\underline{j}}] + \sin\ \alpha\ \hat{\underline{k}}$$

and

$$\hat{\underline{b}}_i = \sin\ \alpha[\sin\ \theta_i\ \hat{\underline{i}} - \cos\ \theta_i\ \hat{\underline{j}}] + \cos\ \alpha\ \hat{\underline{k}}$$

where $\theta_i(z_o)$ is the angle of the center line of the i^{th} strand at z_o.

The equations of motion are then obtained from

$$\frac{d}{dt}\left\{\frac{\partial \mathcal{L}}{\partial \dot{q}}\right\} - \frac{\partial \mathcal{L}}{\partial q} = (\underline{Q}_v + \underline{Q}_c)^T \tag{5.13}$$

where $\mathcal{L} = T - V_s - V_g$. The resulting equations of motion are

$$M_j \ddot{q}_j + d_j \dot{q}_j + K_j\ q_j + \underline{K}_{gj}^T\ \underline{q} = Q_{c_j}$$

where M_j, d_j, and K_j are the generalized mass, damping coefficient and stiffness coefficient, respectively, for the j^{th} vibrational mode. $\underline{K}_{g_j}$ is the j^{th} row of $\underline{\underline{K}}_g$, and Q_{c_j} is the j^{th} element of $\underline{Q}_c$.

Discussion

Complete normal mode analyses have been performed on the finite element models previously discussed. The cases of primary interest are the two seven-strand models. The information acquired from these analyses are twofold. First, the mode shape vectors, $\underline{\phi}_j$ are necessary to define the deformation of the structure in the analytical equations. Figures 5.8-5.9 are typical mode shape plots. Second, the contact forces normal to the strands, f_{ij}, have also been obtained from these analyses.

It has been observed that for several of the vibrational modes, the lower end of the cable, whether free or weighted, has a tendency to separate. When this occurs, the contact forces normal to the strands become negative (i.e., the forces in the springs (scalar elastic elements) become tensile instead of compressive). For these cases, the negative forces are neglected since they would not contribute to Coulomb damping. Another tendency displayed in these analyses is the slipping between strands. Figure 5.10 shows a typical case.

A simulation code has been adopted to perform the "analytical" calculations. The inputs for this code are the mode shape vectors and the contact forces. Results from this code are expected in the next phase of this research.

6. CONCLUSIONS

The phenomena associated with wire rope damping is quite complicated. A macro approximation of it using a uniaxial Coulomb damper with a variable friction force has yielded very good results of isolator response. Various NASTRAN models have been developed which are beginning to provide the kind of analytical capability and insight required for modeling of arbitrary complicated wire rope arrangements. Several other dynamic models have been explored. Beginning experimental studies have shed some light on appropriate wire rope characteristics related to static properties, damping, and dynamic response. Significant progress in deriving closed form solutions for wire rope static properties has been accomplished and their extension to dynamic applications has begun.

7. REFERENCES

Badrakan, "Separation and Determination of Combined Dampings from Free Vibrations," Journal of Sound and Vibration, Vol. 100, No. 2, 1985, pps. 243-255.

Costello, G. A., and Phillips, J. W., "Contact Stresses in Thin Twisted Rods," Journal of Applied Mechanics, Transactions ASME, Series E, Vol. 40, 1973, pps. 629-630.

Costello, G. A., and Phillips, J. W., "Contact Stresses in Thin Twisted Rods," Journal of Applied Mechanics Division, ASCE, Vol. 100, 1974, pps. 1096-1099.

Costello, G. A., and Phillips, J. W., "Effective Modulus of Twisted Wire Cables," Journal of Engineering Mechanics Division, ASCE, Vol. 102, 1976, pps. 171-181.

Craig, R. R., Structural Dynamics, John Wiley and Sons, New York, 1981.

Druckers, D. C., and H. Tachau, "A New Design Criteria for Wire Rope," Journal of Applied Mechanics, Transactions ASME, Vol. 67, 1945, pps. A33-A38.

Gilbert/Commonwealth, Transmission Line Reference Book, Wind-Induced Conductor Motion, Electric Power Research Institute, Palo Alto, CA, 1976.

Huang, N. C., "Finite Extension of an Elastic Strand with a Central Core," Journal of Applied Mechanics, Transactions ASME, Vol. 45, 1978, pps. 852-857.

Jewell, R., NASA/MSFC, Private Communication, December 19, 1984.

Kerley, J., "Concepts and Effects of Damping in Isolators," paper in Rogers (1984), pps. L-1 through L-15.

LeKuch, H. and Silverman, G., "Selecting Shock and Vibration Isolators," Astronautics & Aeronautics, pps. 30-32, September 1983.

Love, A. E. H., A Treatise on the Theory of Elasticity, Dover Publications, Inc., New York, 1944, Chapters 18 and 19.

Meriam, J. L., Dynamics (2nd Ed.), John Wiley, New York, 1975.

Nashif, A. D., Jones, D. I. G., and Henderson, J. P., Vibration Damping, John Wiley & Sons, 1985.

Phillips, J. W., and G. A. Costello, "Contact Stresses in Twisted Wire Cables," Journal of the Engineering Mechanics Division, ASCE, Vol. 99, 1973, pps. 331-341.

Pivovarov, I. and O. G. Vinogradov, "The Phenomenon of Damping in Stranded Cables," Proceedings of the AIAA 26th Structures, Structural Dynamics, and Materials Conference - Part II, April 15-17, 1985, pps. 232-237.

Rogers, L. (Ed.), Vibration Damping 1984 Workshop Proceedings, AFWAL-TR-84-3064, November 1984 (Held at Long Beach, CA, February 1984).

Rogers, L. (Ed.), Damping 1986 Proceedings, AFWAL-TR-86-3059, Vols. 1 and 2, May 1986 (Held at Las Vegas, Nevada, March 1986).

Silverman, J., Aeroflex Lab, Plainview, N. Y., Private Communication, March 22, 1985.

Scoble, W. A., "First Report of the Wire Rope Research Committee," Rochester Institute of Mechanical Engineers, Vol. 115, 1920, pps 835-868; Second Report, Vol. 119, 1924, pps. 1193-1290; Third Report, Vol. 123, 1928, pps. 353-404; Fourth Report, Vol. 130, 1935, pps. 373-478.

Vakakis, A. F. and S. A. Paipetis, "Transient Response of Unidirectional Vibration Isolators with Many Degrees of Freedom," Journal of Sound and Vibration, Vol. 99, No. 4, 1985, pps. 557-562.

8. BIBLIOGRAPHY

Bert, C. W., and R. A. Stein, "Stress Analysis of Wire Rope in Tension and Torsion," Wire and Wire Products, Vol. 37, 1962, pp. 769-770, 772-816.

Chi, M., "Analysis of Multi-Wire Strands in Tension and Combined Tension and Torsion," Developments in Theoretical and Applied Mechanics, Proceedings of the Seventh Southeastern Conference on Theoretical and Applied Mechanics, Vol. 7, 1974, pp. 599-639.

Cochran, J. E., Jr., N. G. Fitz-Coy, and M. A. Cuthins, "Finite Element Models of Wire Rope for Vibration Analysis," presented at the Workshop on Structural Dynamics and Control Interaction of Flexible Structures, Marshall Space Flight Center, Huntsville, Alabama, April 22-24, 1986.

Costello, G. A., "Analytical Investigation of Wire Rope," Applied Mechanics Reviews, pp. 897-900, July 1978. (This was the feature survey article which included 30 references; none address wire rope damping, however.)

Cutchins, M. A., J. E. Cochran, Jr., S. Guest, N. G. Fitz-Coy, and M. L. Tinker, "An Investigation of the Damping Phenomena in Wire Rope Isolators, accepted for ASME Vibrations Conference to be held in Boston, Massachusetts, September 27-30, 1987.

Fabunmi, J. A., "Extended Damping Models for Vibration Data Analysis," Journal of Sound and Vibration, Vol. 101, No. 2, 1985, pp. 181-192.

Ferri, A. A., and E. H. Dowell, "The Behavior of a Linear, Damped Modal System with a Non-Linear Spring-Mass-Dry Friction Damper System Attached, Part I," Journal of Sound and Vibration, 1984.

Ferri, A. A., and E. H. Dowell, The Behavior of a Linear, Damped Model System with a Non-Linear Spring-Mass-Dry Friction Damper System Attached, Part II," Journal of Sound and Vibration, Vol. 101, No. 1, 1985, pp. 55-74.

Hall, H. M., "Stresses in Small Wire Ropes," Wire and Wire Products, Vol. 26, 1951, pp. 228, 257-259.

Harris, C. M., and C. E. Crede, Eds., Shock and Vibration Handbook, 2nd Ed., McGraw-Hill Book Company, Inc., New York, 1976, pp. 32-23 through 32-44 and pp. 36-36 through 36-46.

Hruska, F. H., "Calculations of Stresses in Wire Rope," Wire and Wire Products, Vol. 26, 1951, pp. 766-767, 799-801.

Hruska, F. H., "Radial Forces in Wire Ropes," Wire and Wire Products, Vol. 27, 1952, pp. 459-463.

Hruska, F. H., "Tangential Forces in Wire Ropes," Wire and Wire Products, Vol. 28, 1953, pp. 455-460.

Johnson, C. D., and D. A. Kienholz, "Finite Element Prediction of Damping in Structures with Constrained Viscoelastic Layers," AIAA Journal, Vol. 20, No. 9, September 1982, pp. 1284-1290.

Kumar, K., and J. E. Cochran, Jr., "Analytical Solutions for Static Elastic Deformations of Wire Ropes," accepted for the April 1987 28th AIAA SDM Conference in Monterey, California (AIAA Paper No. 87-0720-CP).

Lazan, Benjamin J., Damping of Materials and Members in Structural Mechanics, Pergamon Press, New York, 1968, pp. 22-23.

Leissa, A. W., "Contact Stresses in Wire Ropes," Wire and Wire Products, Vol. 34, 1959, pp. 307-316, 372-373.

Machida, S., and A. J. Durelli, "Response of a Strand to Axial and Torsional Displacements," Journal of Mechanical Engineering Science, Vol. 15, 1973, pp. 241-251.

Phillips, J. W., and G. A. Costello, "Analysis of Wire Ropes with Internal-Wire-Rope Cores," Journal of Applied Mechanics, Vol. 52, No. 3, 1985, pp. 510-516.

Rogers, L. C., and K. E. Richards, Jr., "PACOSS Program Overview and Status," pp. 85-109 of Wright (1986).

Ruzicka, J. E., and T. F. Derby, Influence of Damping in Vibration Isolation, the Shock and Vibration Information Center, Naval Research Laboratory, Washington, D. C., 1971.

Santini, P., A. Casteilani and A. Nappi, "An Introduction to the Problem of Dynamic Structural Damping," AGARD Report No. 663, January 1978.

Sayers, D. D., and M. C. Potter, "The Effects of Curvature and Torsion on the Temperature Distribution in a Helix," Journal of Applied Mechanics, Vol. 52, No. 3, 1985, pp. 529-532.

Starkey, W. L., and H. A. Cress, "An Analysis of Critical Stresses and Mode of Failure of a Wire Rope," Journal of Engineering for Industry, Transactions, ASME, Vol. 81, 1959, pp. 307-316.

Vinogradov, O. G., and I. S. Atatekin, "Internal Friction Due to Wire Twist in Bent Cable," Journal of Engineering Mechanics, Vol. 112, No. 9, pp. 859-873, 1986.

Vinogradov, O. G., and I. S. Atatekin, "Structural Damping of Stranded Cable," Mathematical Modeling in Service and Technology, Pergamon Press, Avula, X., et al. (Eds.), pp. 537-541, 1984.

Wright, R. L. (Ed.), NASA/DOD Control/Structures Interaction Technology, NASA CP 2447, Part I, Proceedings of a conference held in Norfolk, VA, November 15-21, 1986.

_____, American Wire Rope, American Steel and Wire Company, New York, 1913.

_____, Vibration Damping Short Course Notes, University of Dayton Research Institute, June 1983.

ORIGINAL PAGE IS
OF POOR QUALITY

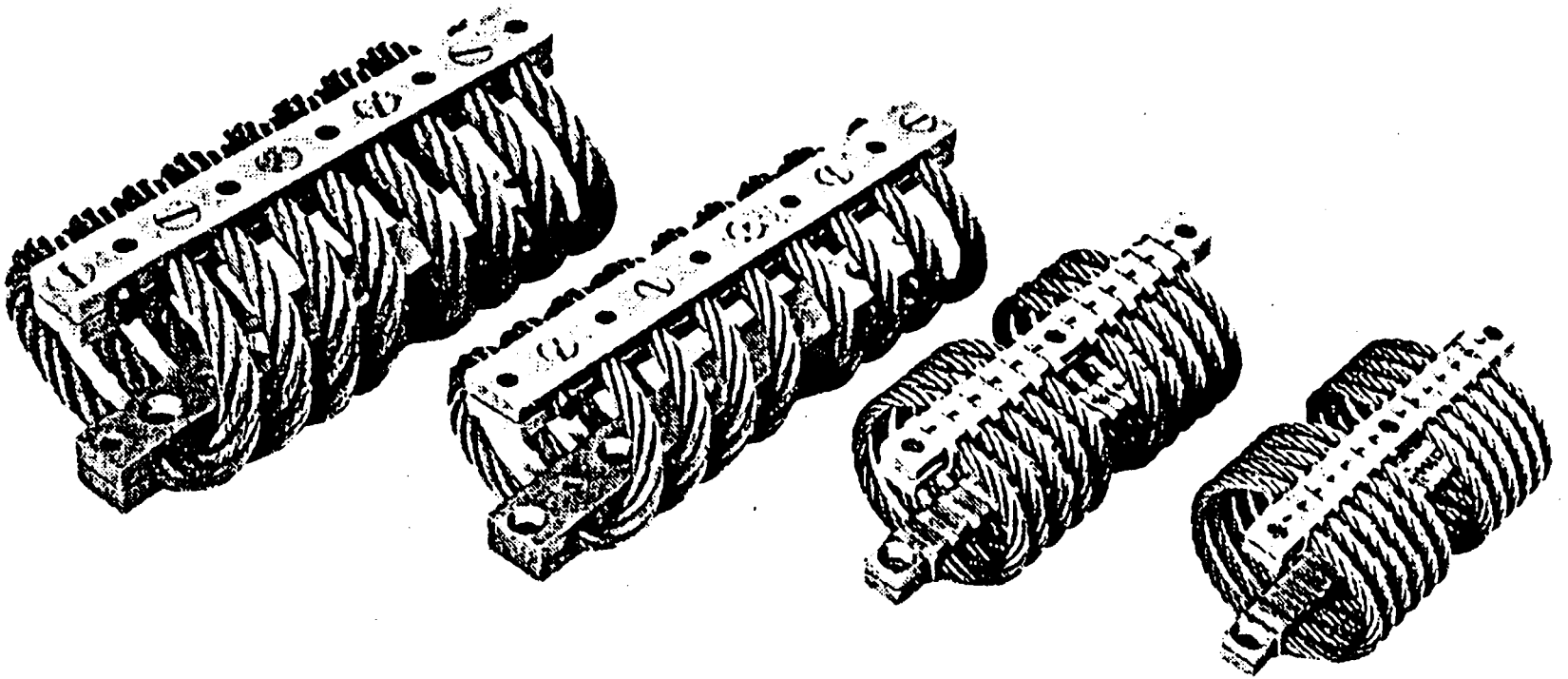

Fig. 1.1 Helical isolators.

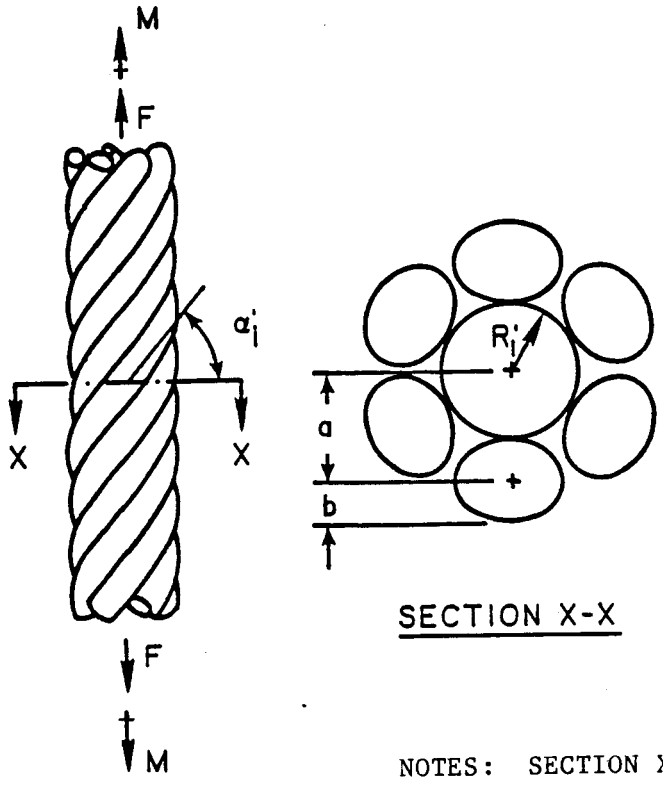

NOTES: SECTION X-X

FOR ROPE WITH FIBROUS CORE
HELICAL WIRES CONTACT

$a = r \qquad b = R$

FOR ROPE WITH METALLIC CORE
HELICAL WIRES DO NOT CONTACT (SHOWN)

$a = r_i \qquad b = R_i'$

Fig. 3.1 Rope geometry with $m_2 = 6$ and $m_1 = 1$.

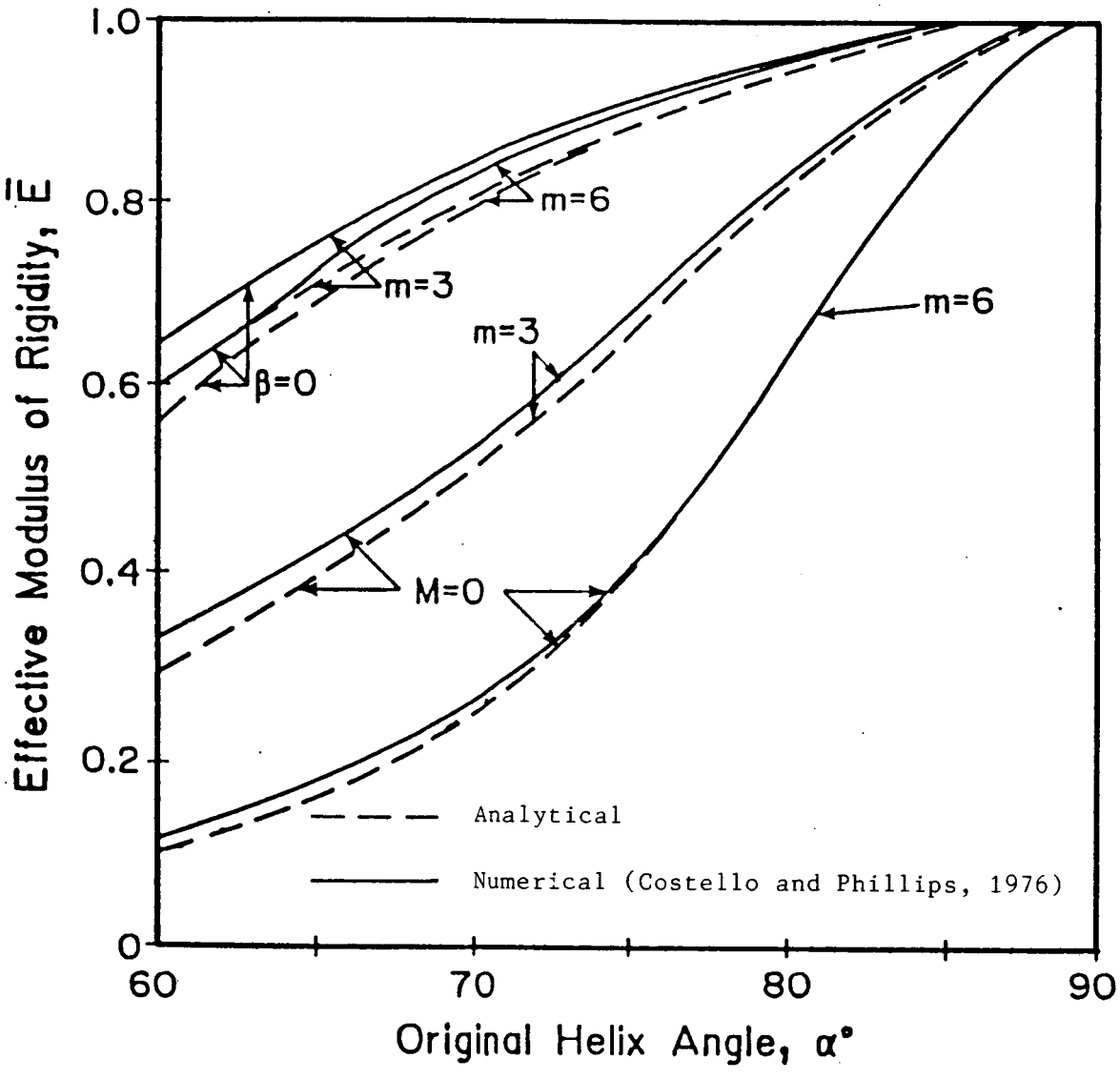

Fig. 3.2 Plots comparing the analytical and numerical values of effective modulus of rigidity of wire rope for the practical range of α.

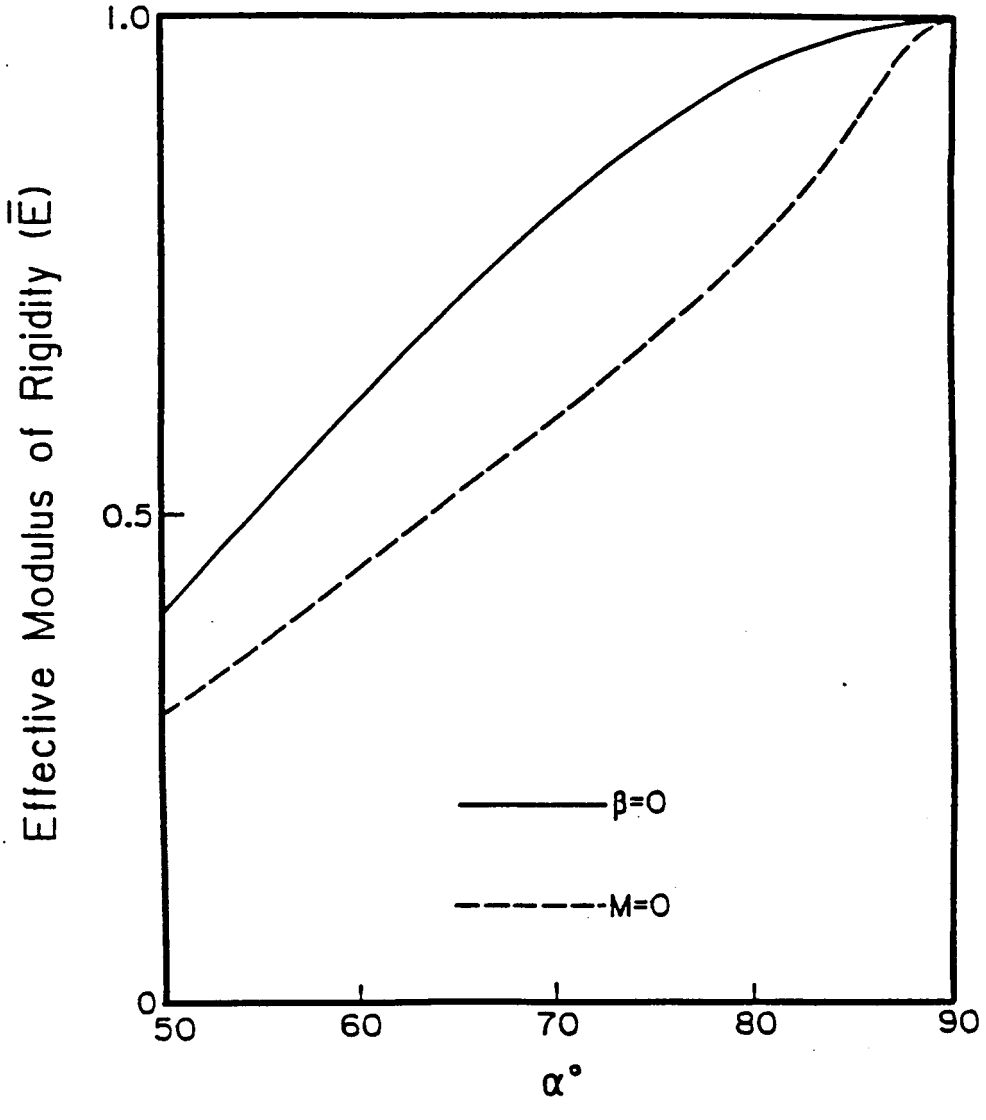

Fig. 3.3 Modulus of Rigidity as affected by the helix angle.

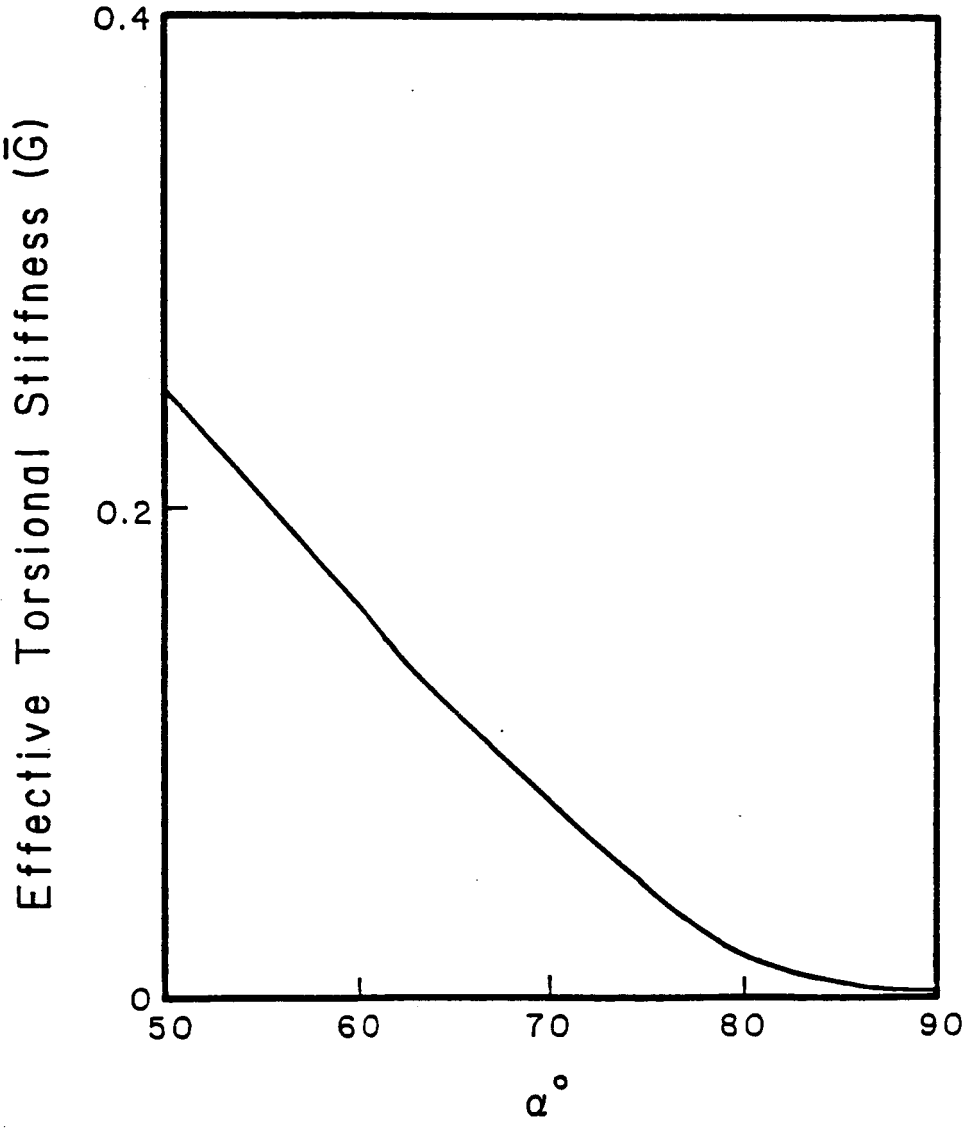

Fig. 3.4 Torsional Stiffness as affected by the helix angle.

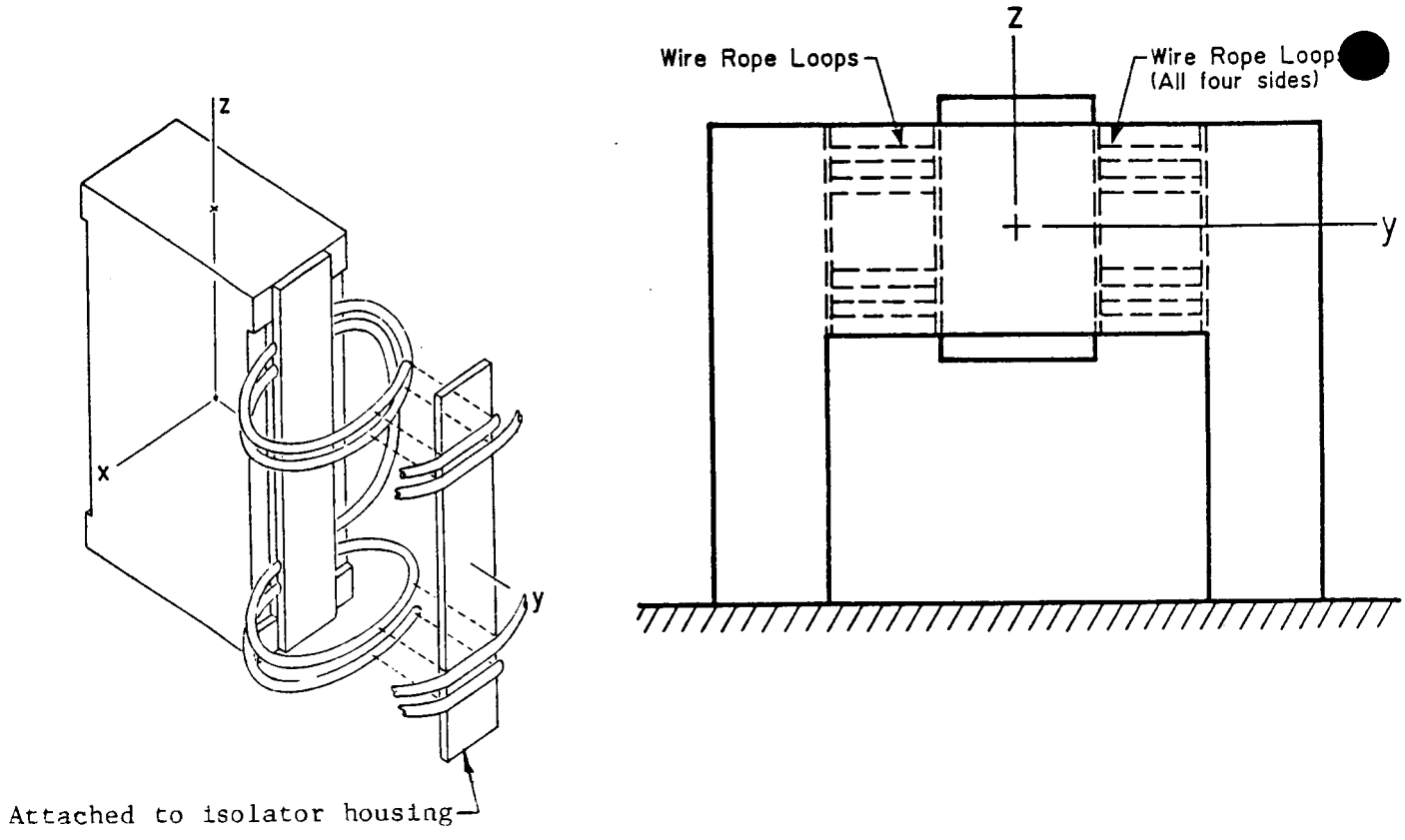

(a) Partial isometric

(b) Side view

Figure 4.1 Wire rope vibration isolator.

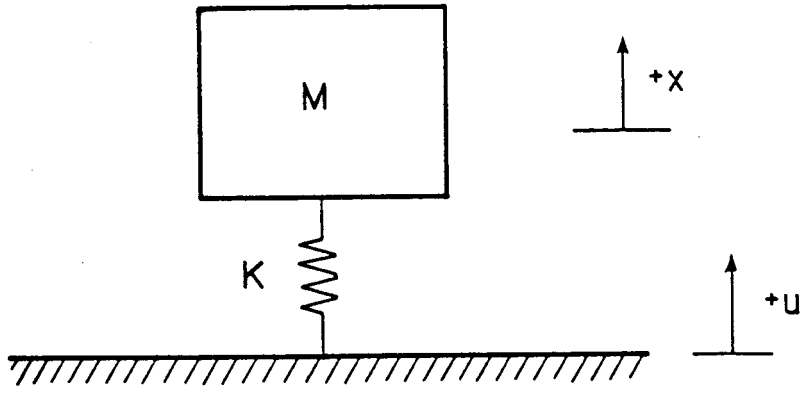

Figure 4.2 Undamped single-degree-of-freedom model.

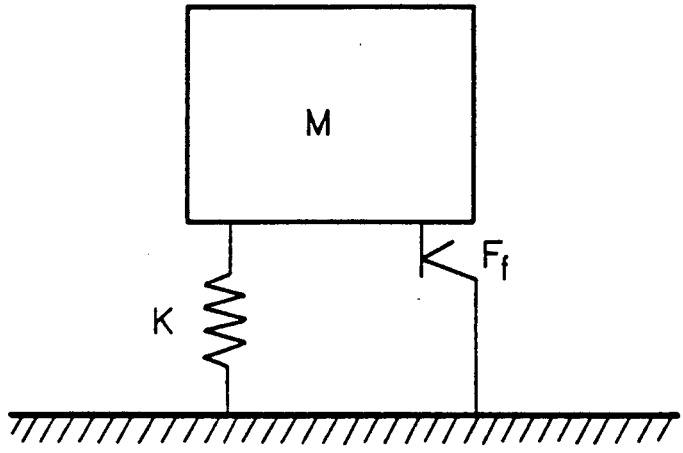

Figure 4.3 Rigidly connected Coulomb damper model.

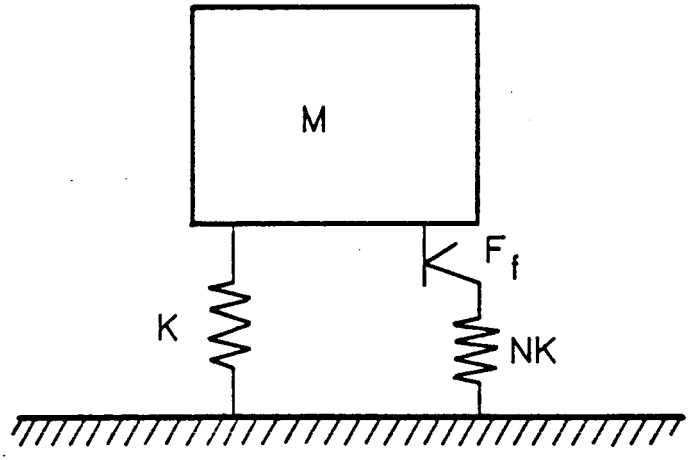

Figure 4.4 Elastically connected Coulomb damper model.

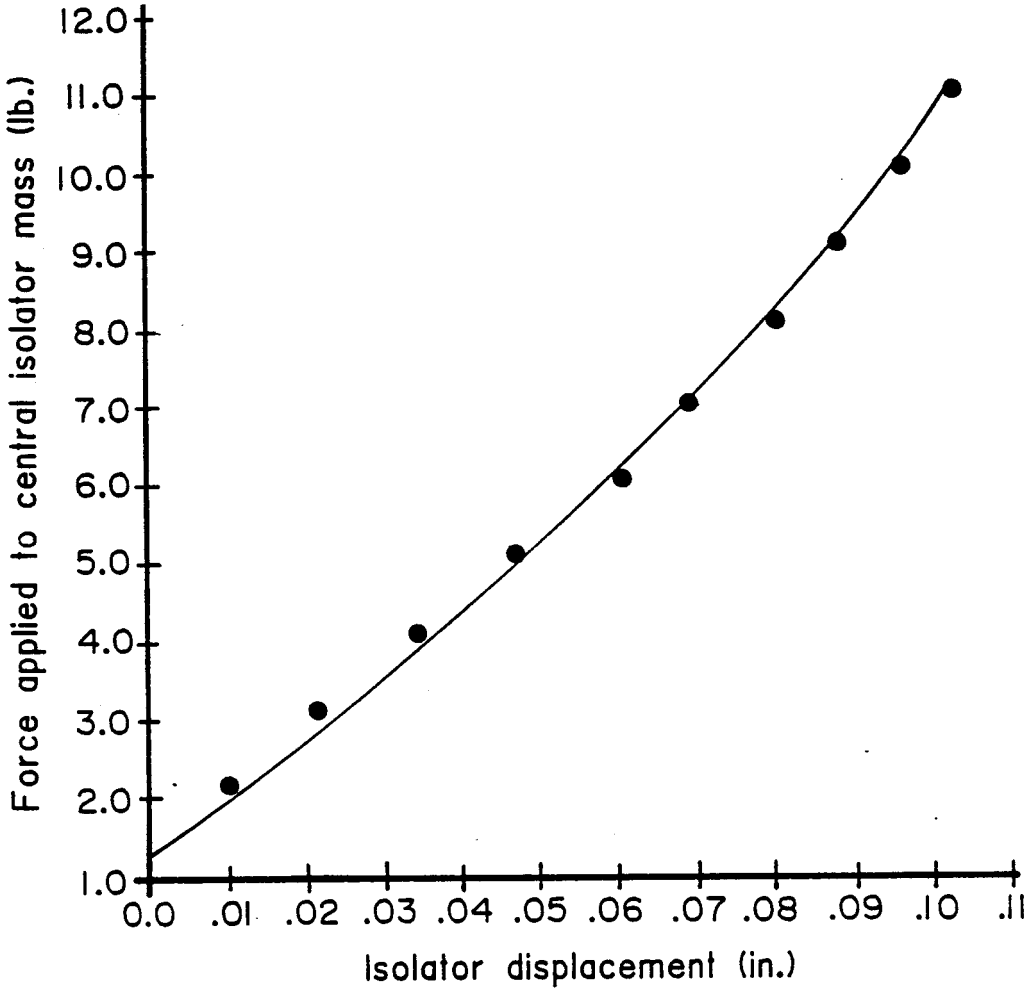

Fig. 4.5 Isolator force versus displacement curve.

```
PROGRAM ISOL
  INITIAL
    CONSTANT   MASS=.1359    ,   G=386.4    ,   SLOPE=97.656
    CONSTANT   N=0.0         ,  OMEGA=40.0  ,   UZERO=.0840
    CONSTANT   TDEL=0.0      ,   PI=3.1416  ,   PHASE=0.0
    CONSTANT   TSTOP= 6.0    ,   XO=0.0     ,   XDO=0.0
    TABLE FF, 1, 14
          /    10.0,   20.0,   40.0,   60.0,   70.0 ...
          ,    75.0,   80.0,  100.0,  120.0,  140.0 ...
          ,   160.0,  180.0,  200.0,  250.0          ...
          ,    0.75,   0.85,   1.25,   0.15,   0.10 ...
          ,    0.10,   2.25,   1.45,   0.50,  0.005 ...
          ,   0.007,  0.007,  0.004,  0.004           /
    CINTERVAL  CINT=0.002
  END $ 'OF INITIAL'
      DYNAMIC
        W = 2.*PI*OMEGA
          DERIVATIVE
            F1 = UZERO*HARM(TDEL,W,PHASE)
            XDD = -G/MASS*(SLOPE*(X-F1) + FF(OMEGA)*SIGN(1.0,XD))
            XD = INTEG(XDD,XDO)
            X = INTEG(XD,XO)
          END $ 'OF DERIVATIVE'
          TERMT(T.GT.TSTOP)
      END $ 'OF DYNAMIC'
END $ 'OF PROGRAM'
```

Fig. 4.6 Listing of ACSL program for Coulomb friction model with variable friction force.

TABLE I. ISOLATOR VIBRATION TEST DATA

Run 2 Vertical

Frequency (H_z)	Base Peak Accel. (g's)	Base Disp. (in.)	Mass Peak Accel. (g's)	Mass Disp. (in.)	Relative Disp. (in.)
10	1.1	0.302	1.1	0.309	.0070
20	2.9	0.170	3.0	0.180	.0100
40	6.1	0.084	7.7	0.103	.0190
60	8.3	0.051	18.5	0.113	.0620
70	7.6	0.033	40.1	0.181	.1480
75	7.6	0.028	50.6	0.191	.1630
80	10.2	0.034	31.3	0.105	.0710
84		≈ 0.032			
100	12.3	0.024	15.5	0.030	.0060
120	12.45	0.016	11.45	0.014	-.002
140	12.6	0.012	9.6	0.012	-.004
160	12.7	0.008	8.2	0.004	-.004
180	12.6	0.006	7.1	0.002	-.004
200	12.2	0.004	6.3	0.003	-.001
250	11.8	0.0025	5.6	0.0003	.0005
300	11.1	-	4.3	-	-

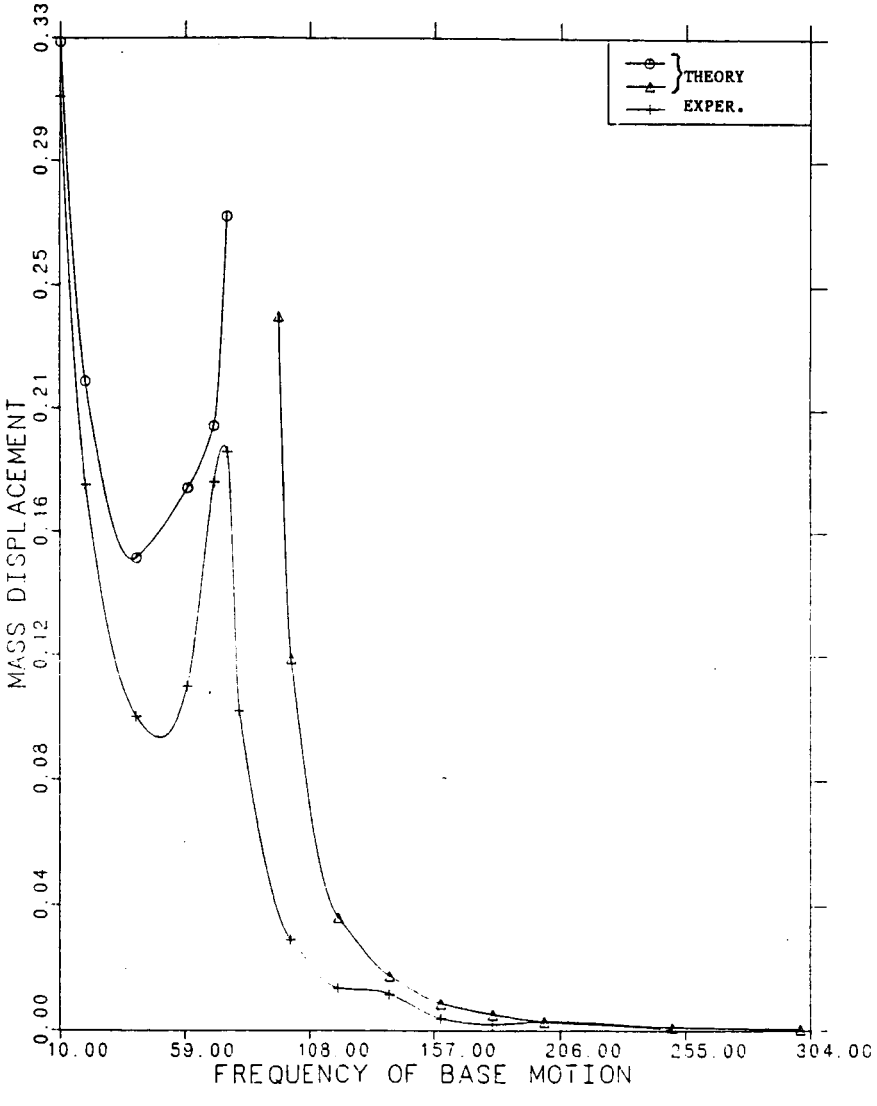

Fig. 4.7 Theory (undamped model) vs. experiment.

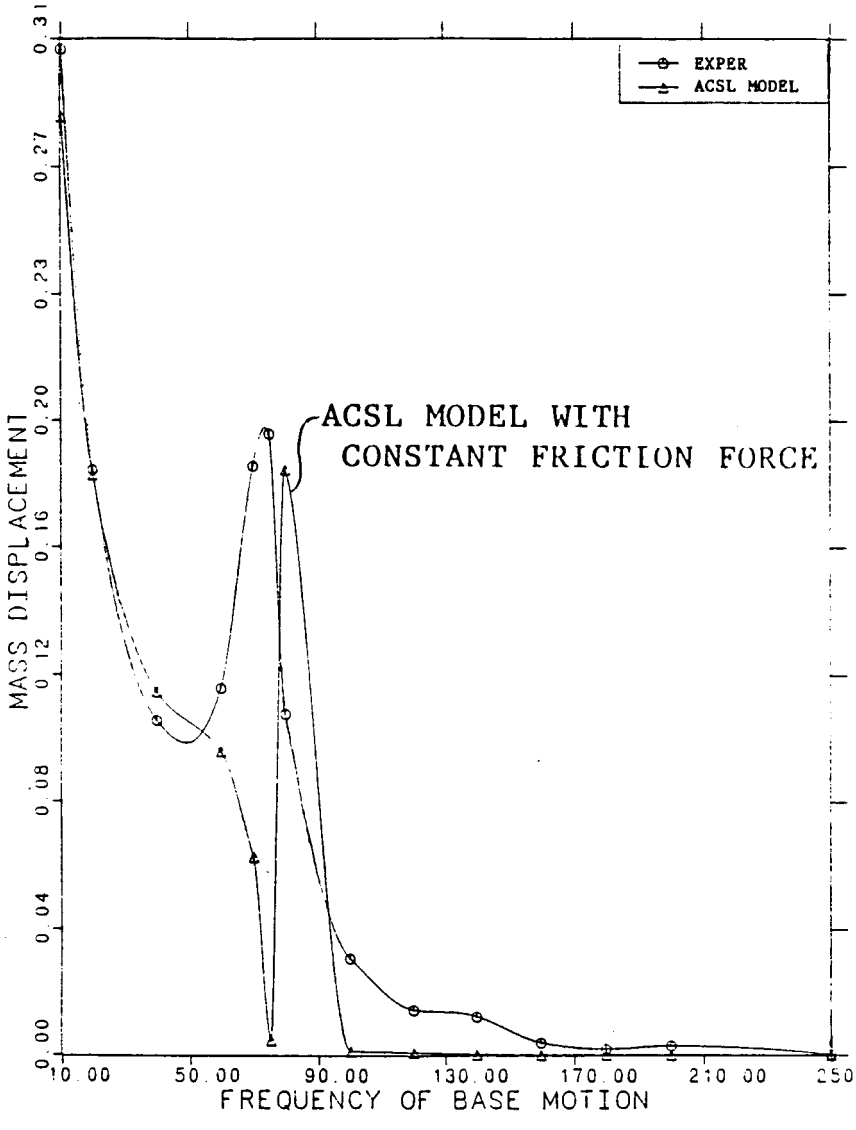

Fig. 4.8 Theory (Coulomb model with constant friction force) vs. experiment.

TABLE II. ONE POSTULATED VARIATION OF FRICTION FORCE WITH FREQUENCY.

Frequency (Hz)	F_f (lb)
10	0.75
20	0.85
40	1.25
60	0.15
70	0.10
75	0.10
80	2.25
100	1.45
120	0.50
140	0.005
160	0.007
180	0.007
200	0.004
250	0.004

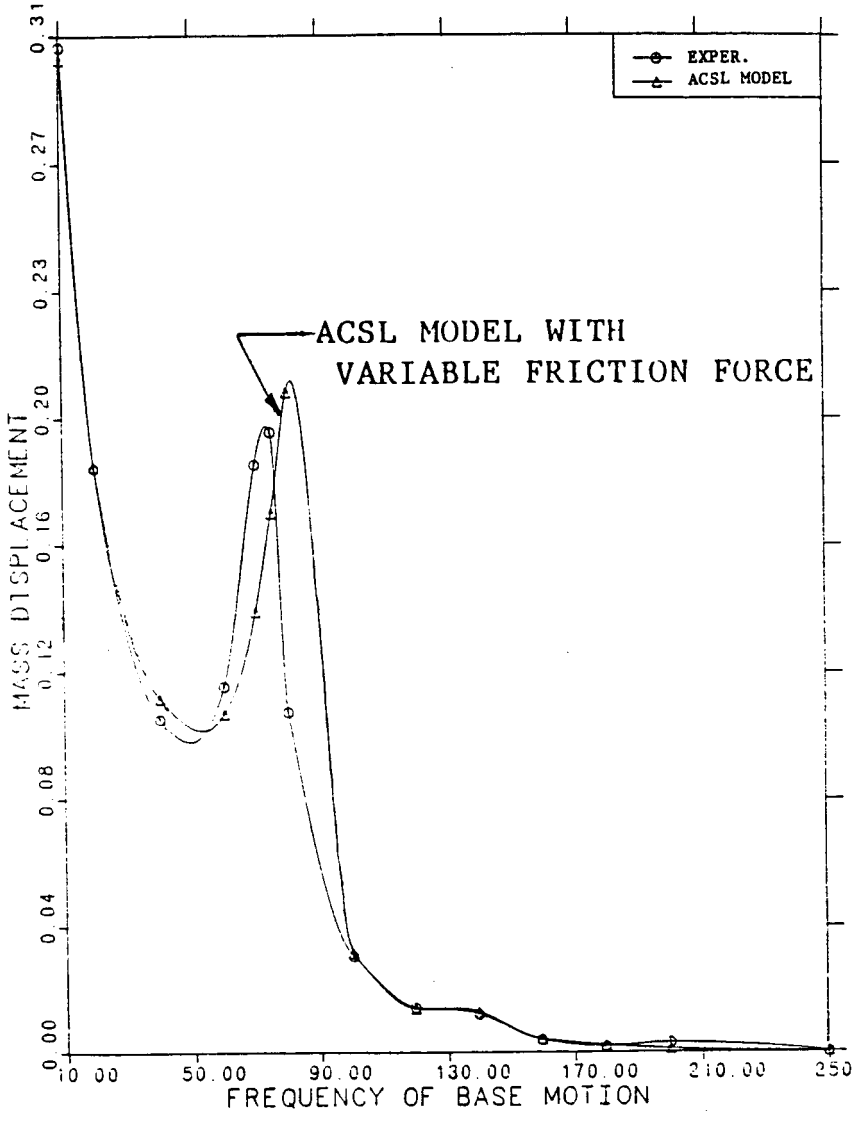

Fig. 4.9 Theory (Coulomb model with variable friction force) vs. experiment.

ORIGINAL PAGE IS
OF POOR QUALITY

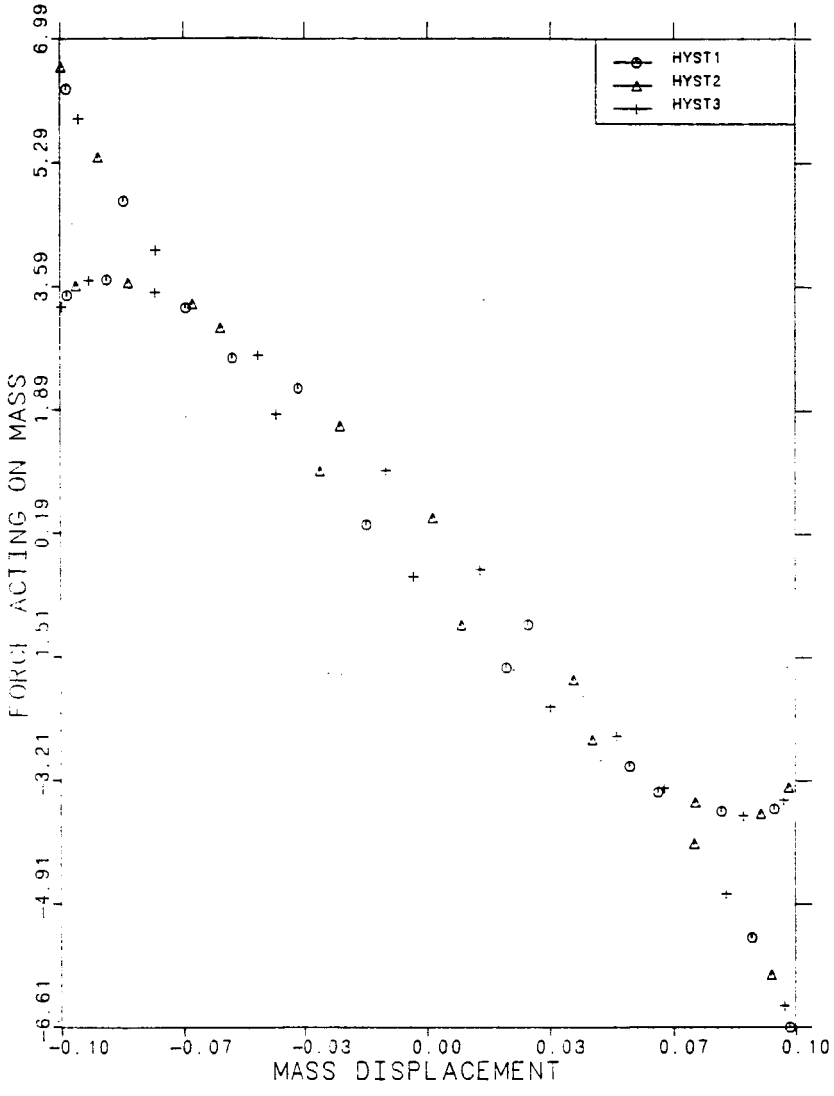

Fig. 4.10 ACSL-generated 60 Hz hysteresis loop.

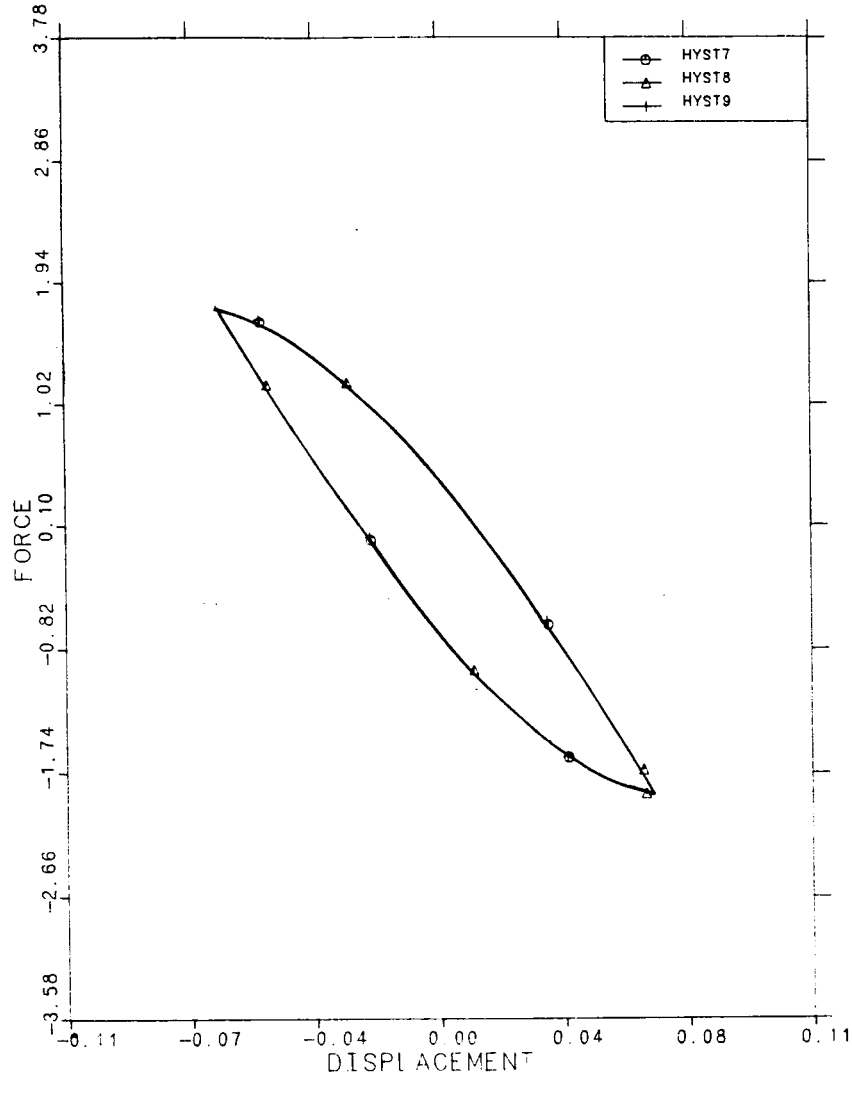

Fig. 4.10 (Cont.) ACSL-generated 40 Hz hysteresis loop.

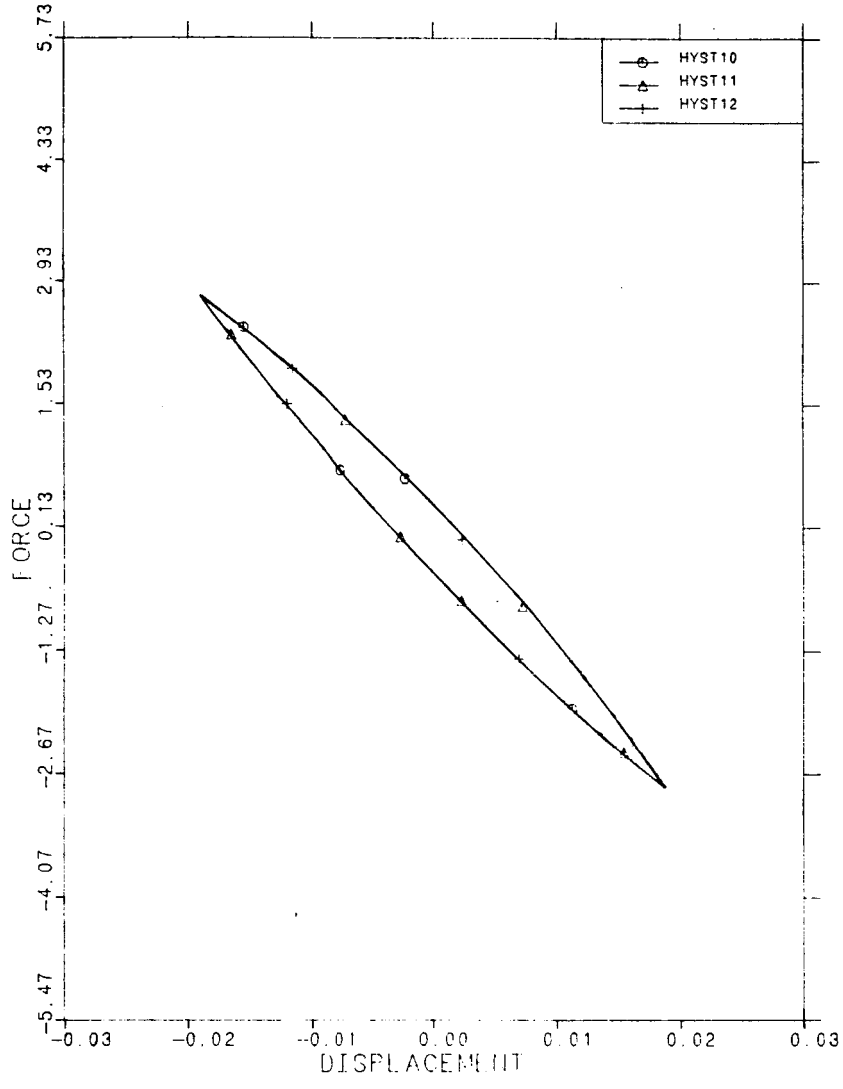

Fig. 4.10 (Cont.) ACSL-generated 100 Hz hysteresis loop.

TABLE III. NASTRAN SINGLE LOOP MODEL

```
ID WIRE ROPE ISOLATOR SINGLE LOOP LINE ELEMENT MODEL
TIME 100
SOL 24
CEND
TITLE=WIRE ROPE ISOLATOR SINGLE LOOP LINE ELEMENT MODEL
SUBTITLE=   1.25" MAJOR AXIS AND 1.125" MINOR AXIS
LABEL= STATIC LOADING MODEL
ECHO=BOTH
SET 10 =1,76,51
DISPLACEMENT=10
SUBCASE 1
LABEL= .302 LB STATIC LOADING
LOAD= 101
SUBCASE 2
LABEL= .652 LB STATIC LOADING
LOAD= 102
SUBCASE 3
LABEL= .852 LB STATIC LOADING
LOAD= 103
SUBCASE 4
LABEL= 1.052 LB STATIC LOADING
LOAD= 104
$OUTPUT(PLOT)
$PLOTTER NAST
$SET 1 =ALL
$VIEW 0.,0.,0.
$AXES Z,X,Y
$FIND SCALE ORIGIN 0, SET 1
$PTITLE=WIRE ROPE ISOLATOR SINGLE LOOP LINE ELEMENT MODEL
$PLOT SET 1, ORIGIN 0, SET 1
BEGIN BULK
GRID,1,,-1.25,0.0,0.0,,
GRID,2,,-1.20,.315,0.0,,
GRID,3,,-1.15,.440908,0.0,,
GRID,4,,-1.10,.5343454,0.0,,
GRID,5,,-1.05,.6104097,0.0,,
GRID,6,,-1.00,.675,0.0,,
GRID,7,,-.95,.7311635,0.0,,
GRID,8,,-.9,.7807208,0.0,,
GRID,9,,-.85,.8248636,0.0,,
GRID,10,,-.80,.8644218,0.0,,
GRID,11,,-.75,.9,0.0,,
GRID,12,,-.70,.9320542,0.0,,
GRID,13,,-.65,.960937,0.0,,
GRID,14,,-.60,.986827,0.0,,
GRID,15,,-.55,1.010248,0.0,,
GRID,16,,-.50,1.031080,0.0,,
GRID,17,,-.45,1.049571,0.0,,
GRID,18,,-.40,1.065845,0.0,,123456
GRID,19,,-.35,1.08,0.0,,123456
```

```
GRID,20,,-.30,1.092120,0.0,,123456
GRID,21,,-.25,1.102270,0.0,,123456
GRID,22,,-.20,1.110507,0.0,,123456
GRID,23,,-.15,1.116871,0.0,,123456
GRID,24,,-.10,1.12139,0.0,,123456
GRID,25,,-.05,1.124100,0.0,,123456
GRID,26,,0.0,1.125,0.0,,123456
GRID,51,,1.25,0.0,0.0,,
GRID,50,,1.20,.315,0.0,,
GRID,49,,1.15,.440908,0.0,,
GRID,48,,1.10,.5343454,0.0,,
GRID,47,,1.05,.6104097,0.0,,
GRID,46,,1.00,.675,0.0,,
GRID,45,,.95,.7311635,0.0,,
GRID,44,,.9,.7807208,0.0,,
GRID,43,,.85,.8248636,0.0,,
GRID,42,,.80,.8644218,0.0,,
GRID,41,,.75,.9,0.0,,
GRID,40,,.70,.9320542,0.0,,
GRID,39,,.65,.960937,0.0,,
GRID,38,,.60,.986827,0.0,,
GRID,37,,.55,1.010248,0.0,,
GRID,36,,.50,1.031080,0.0,,
GRID,35,,.45,1.049571,0.0,,
GRID,34,,.40,1.065845,0.0,,123456
GRID,33,,.35,1.08,0.0,,123456
GRID,32,,.30,1.092120,0.0,,123456
GRID,31,,.25,1.102270,0.0,,123456
GRID,30,,.20,1.110507,0.0,,123456
GRID,29,,.15,1.116871,0.0,,123456
GRID,28,,.10,1.12139,0.0,,123456
GRID,27,,.05,1.124100,0.0,,123456
GRID,52,,1.20,-.315,0.0,,
GRID,53,,1.15,-.440908,0.0,,
GRID,54,,1.10,-.534345,0.0,,
GRID,55,,1.05,-.610410,0.0,,
GRID,56,,1.00,-.675,0.0,,
GRID,57,,.95,-.731164,0.0,,
GRID,58,,.9,-.780721,0.0,,
GRID,59,,.85,-.824864,0.0,,
GRID,60,,.80,-.864422,0.0,,
GRID,61,,.75,-.9,0.0,,
GRID,62,,.70,-.932054,0.0,,
GRID,63,,.65,-.960937,0.0,,
GRID,64,,.60,-.986827,0.0,,
GRID,65,,.55,-1.01025,0.0,,
GRID,66,,.50,-1.03108,0.0,,
GRID,67,,.45,-1.04957,0.0,,
GRID,68,,.40,-1.06585,0.0,,12456
GRID,69,,.35,-1.08,0.0,,12456
GRID,70,,.30,-1.09212,0.0,,12456
```

```
GRID,71,,.25,-1.10227,0.0,,12456
GRID,72,,.20,-1.11051,0.0,,12456
GRID,73,,.15,-1.11687,0.0,,12456
GRID,74,,.10,-1.12139,0.0,,12456
GRID,75,,.05,-1.12410,0.0,,12456
GRID,76,,0.0,-1.125,0.0,,12456
GRID,100,,-1.20,-.315,0.0,,
GRID,99,,-1.15,-.440908,0.0,,
GRID,98,,-1.10,-.534345,0.0,,
GRID,97,,-1.05,-.61041,0.0,,
GRID,96,,-1.00,-.675,0.0,,
GRID,95,,-.95,-.731164,0.0,,
GRID,94,,-.9,-.780721,0.0,,
GRID,93,,-.85,-.824864,0.0,,
GRID,92,,-.80,-.864422,0.0,
GRID,91,,-.75,-.9,0.0,,
GRID,90,,-.70,-.932054,0.0,,
GRID,89,,-.65,-.960937,0.0,,
GRID,88,,-.60,-.986827,0.0,,
GRID,87,,-.55,-1.01025,0.0,,
GRID,86,,-.50,-1.03108,0.0,,
GRID,85,,-.45,-1.04957,0.0,,
GRID,84,,-.40,-1.06585,0.0,,12456
GRID,83,,-.35,-1.08,0.0,,12456
GRID,82,,-.30,-1.09212,0.0,,12456
GRID,81,,-.25,-1.10227,0.0,,12456
GRID,80,,-.20,-1.11051,0.0,,12456
GRID,79,,-.15,-1.11687,0.0,,12456
GRID,78,,-.10,-1.12139,0.0,,12456
GRID,77,,-.05,-1.12410,0.0,,12456
FORCE,101,76,,.302,0.0,0.0,1.0
FORCE,102,76,,.652,0.0,0.0,1.0
FORCE,103,76,,.852,0.0,0.0,1.0
FORCE,104,76,,1.052,0.0,0.0,1.0
CBAR,1,35,1,2,0.0,1.0,0.0
=,*(1),=,*(1),*(1),==
=97
CBAR,100,35,100,1,0.0,1.0,0.0
PBAR,35,75,0.013829,1.95312-5,1.95312-5,3.90648-5
MAT1,75,30.+5,11.54+5,,7.324-4
PARAM,GRDPNT,1
PARAM,WTMASS,0.0025907
ENDDATA
```

ORIGINAL PAGE IS
OF POOR QUALITY

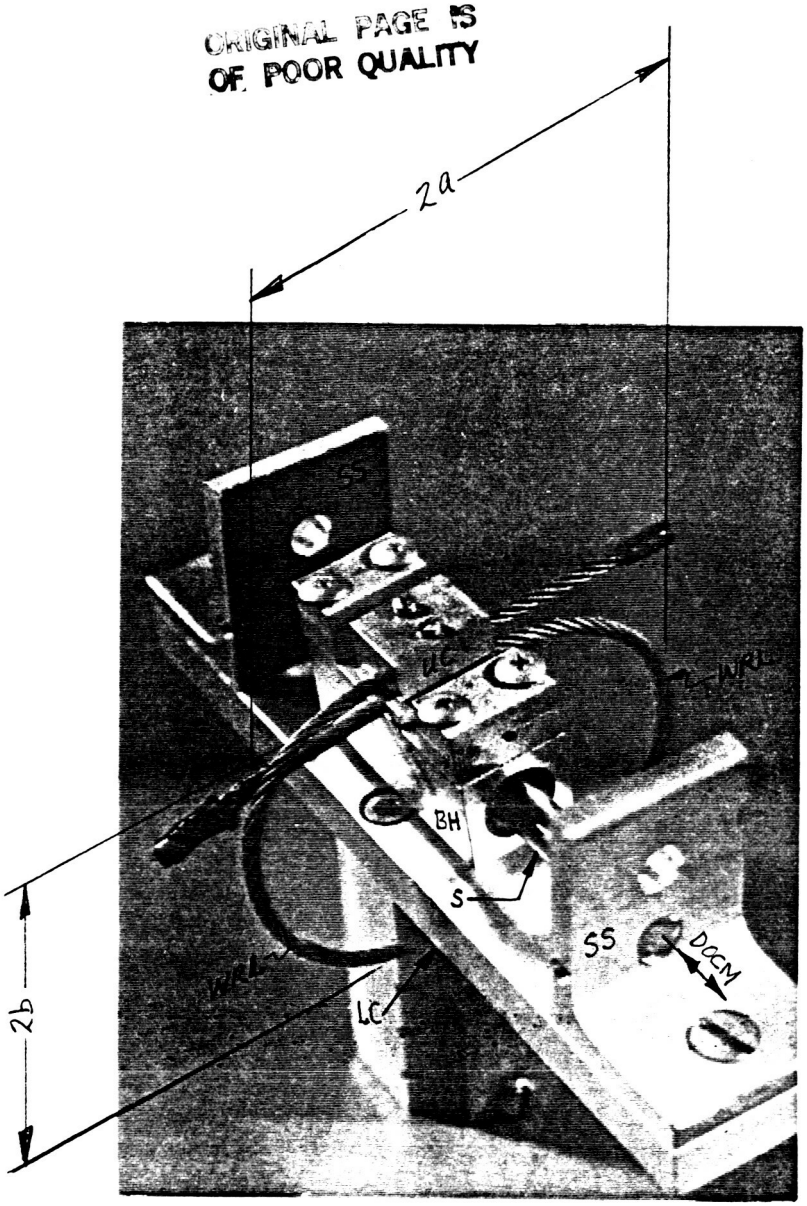

BH = Bearing Housing
DOCM = Direction of Constrained Motion (of BH & UC)
LC = Lower Clamp
S = Shaft (fixed in both SS's)
SS = Shaft Support
UC = Upper Clamp
WRL = Wire Rope Loop

Fig. 4.11 Single loop wire rope experimental arrangement.

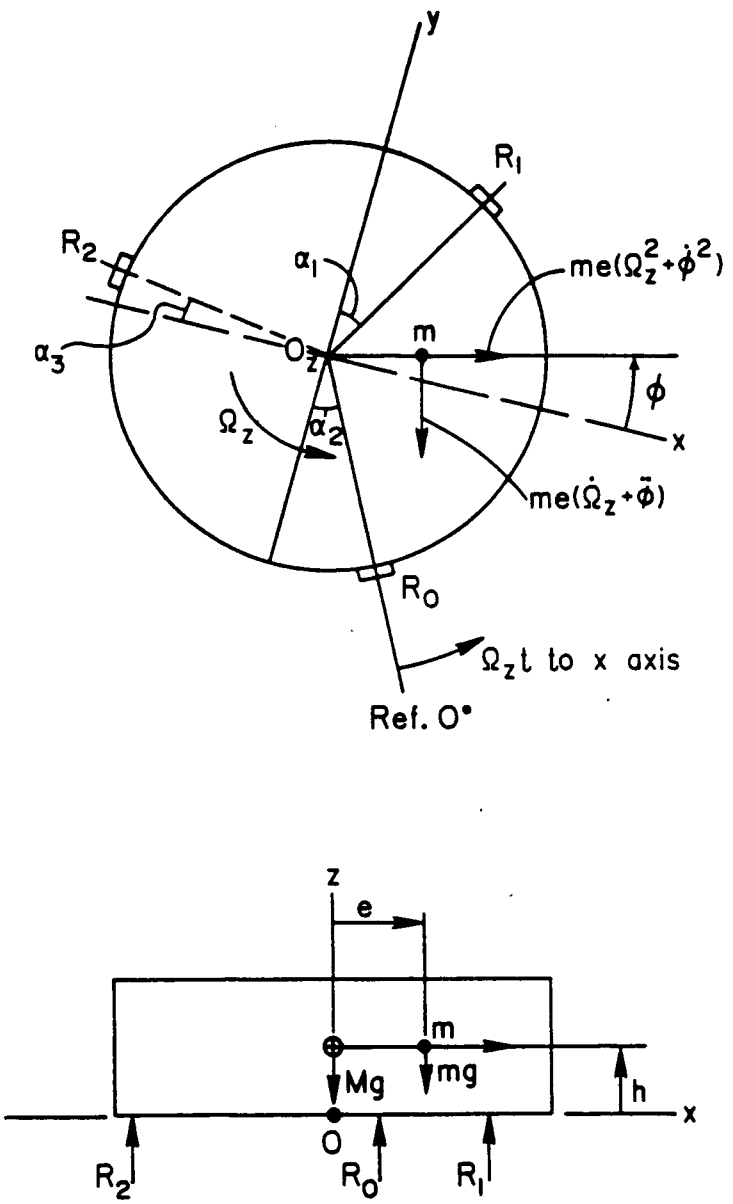

Figure 4.12 Momentum wheel with three isolator support pairs.

```
PROGRAM
MACRO ISOPAIR(N)

  "ONE-DIMENSIONAL COULOMB FRICTION MODEL W/VARIABLE FRICTION"
  "e.g., MOST OF FIG. 4.6 CODING SLIGHTLY MODIFIED"

S

MACRO END
ARRAY I(3)
CONSTANT      "INPUT OF M,e,R,K's,h,m,INITIAL CONDS."

INITIAL
 "COMPUTATION OF IXX,IYY,IZZ, AND m x e"
 "CONVERSION OF IC'S TO RADIANS AND RAD./SEC."
END
DYNAMIC

DERIVATIVE

  "ROTATIONAL EQS. FOR MOMENTUM WHEEL W/3 SYMM.-SPACED, PAIRED
     ISOLATORS"

  "FUNCTION OF MASS, e, I'S, α's, Ω's, Ω̇'s, φ̇, φ̈, R AND 3 ISOLATORS"

  MZ = f(T)
  {Ω} = ∫{Ω̇}dt

  {θ} = ∫{Ω}dt
  φ̇ = ∫φ̈ dt
  φ = ∫ φ̇ dt
S

  ISOPAIR(1)
  ISOPAIR(2)      INVOCATION OF MACRO'S
  ISOPAIR(3)

  {α} = {g(t,Ωz)}

   THETMAX = SQRT(θX**2 + θY**2 + φ**2) $ "A MEASURE OF ISOLATION"

END $ "OF DERIV"

 END $ "OF DYNAM"

END $ "OF PROGRAM"
```

Figure 4.13. ACSL model definition arrangement - wire rope isolated momentum wheel ([← S →] denotes sorted sections).

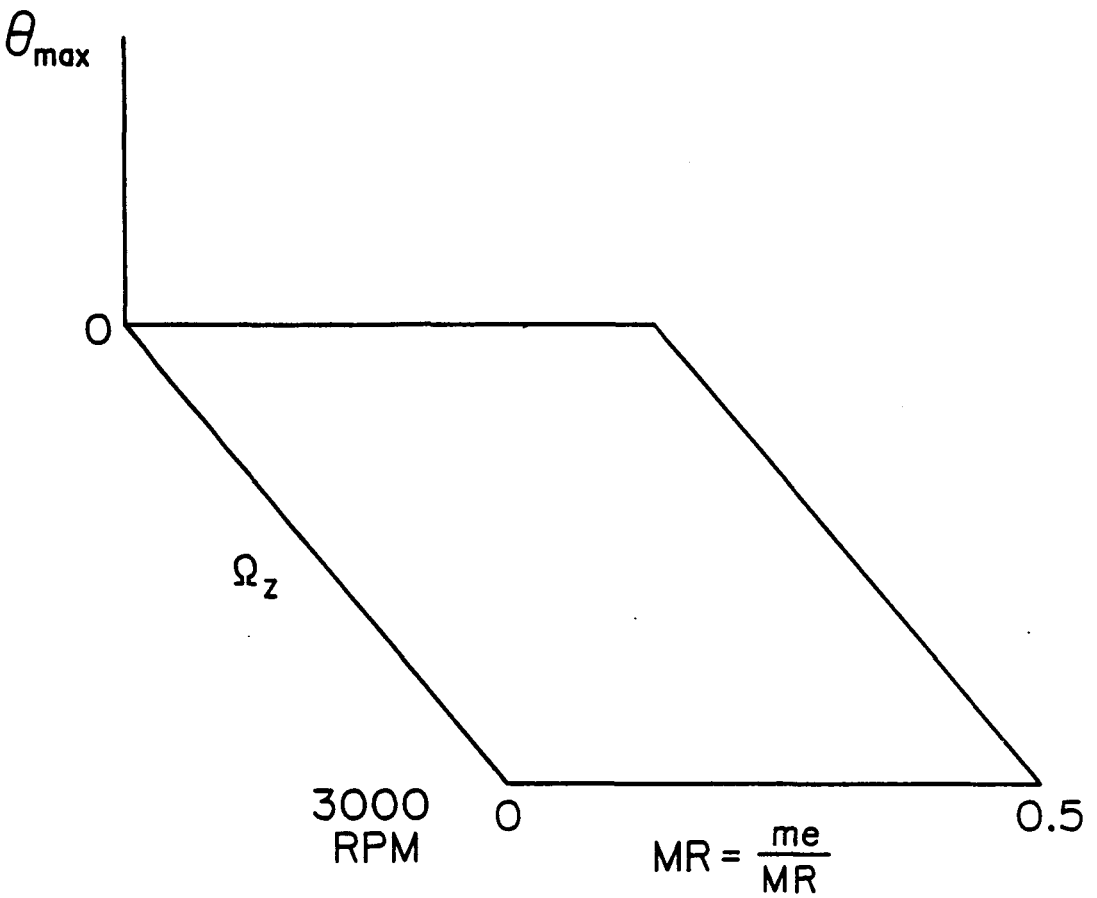

Figure 4.14 Planned output arrangement for isolator-supported investigation.

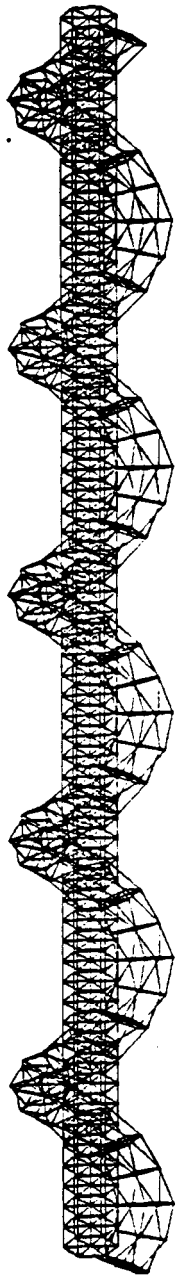

Fig. 5.1. NASTRAN model of two-strand wire rope.

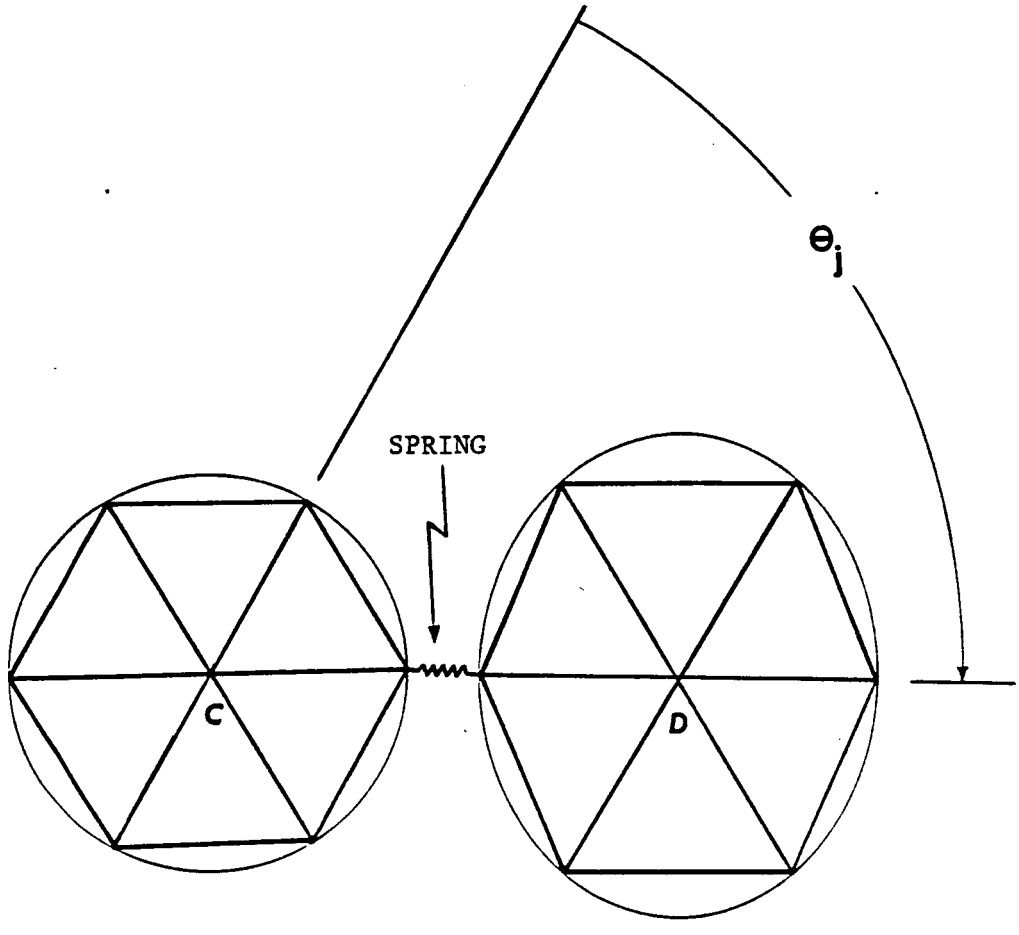

Fig. 5.2 Cross section of two-strand wire rope showing finite elements.

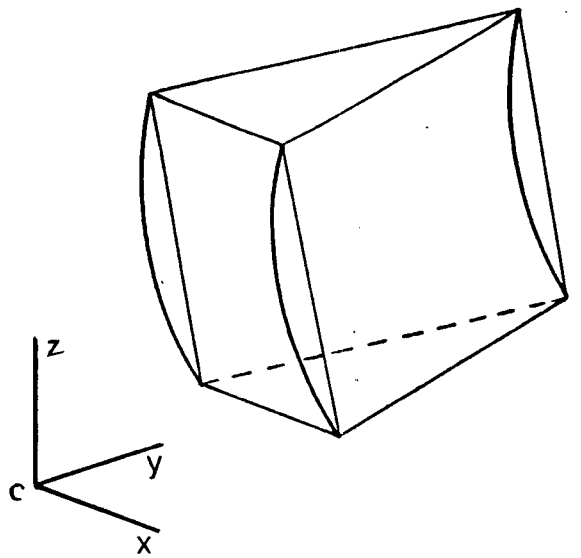

Fig. 5.3. PENTA MSC/NASTRAN solid element.

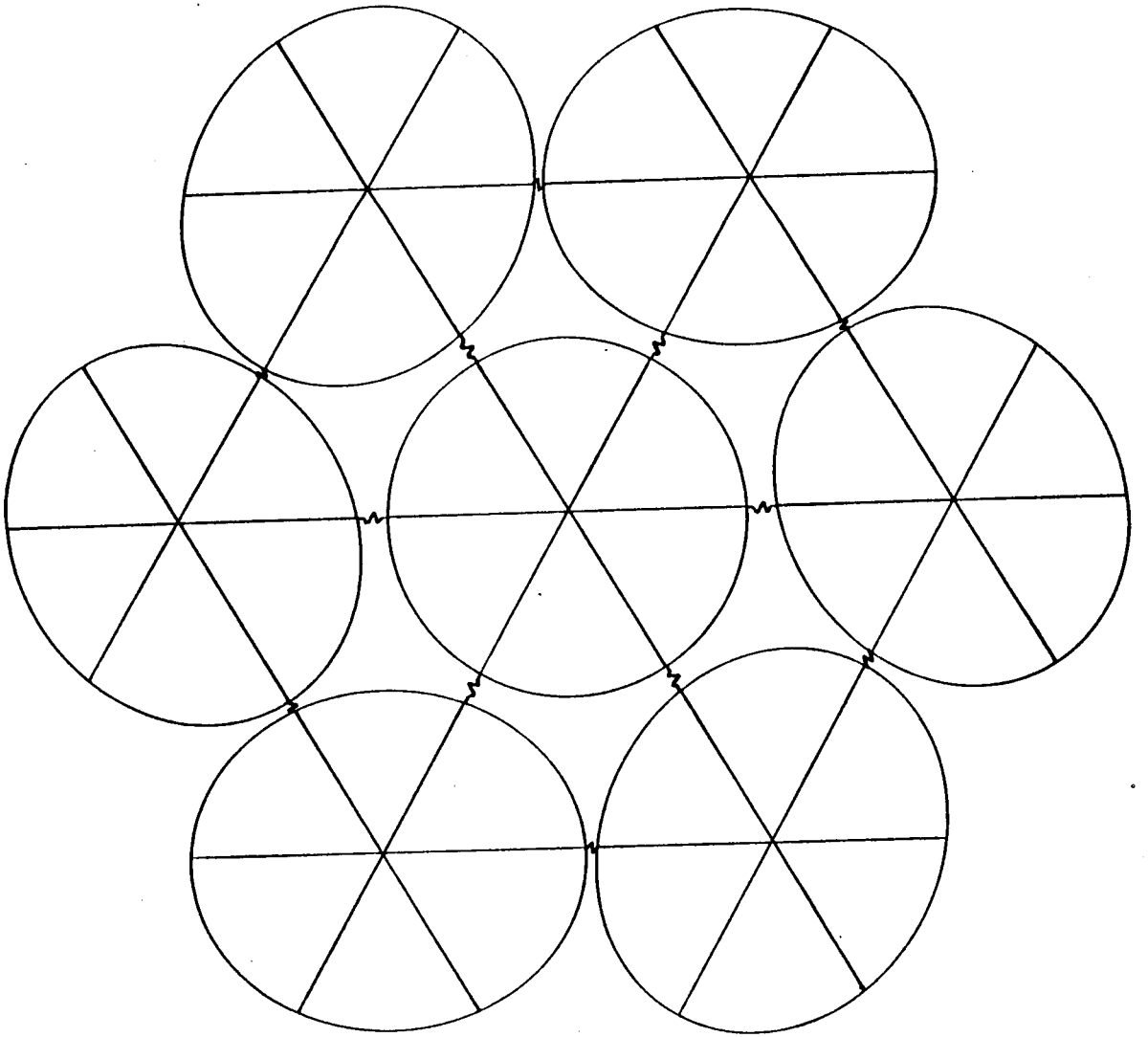

Fig. 5.4. Cross section of seven-strand wire rope showing finite elements.

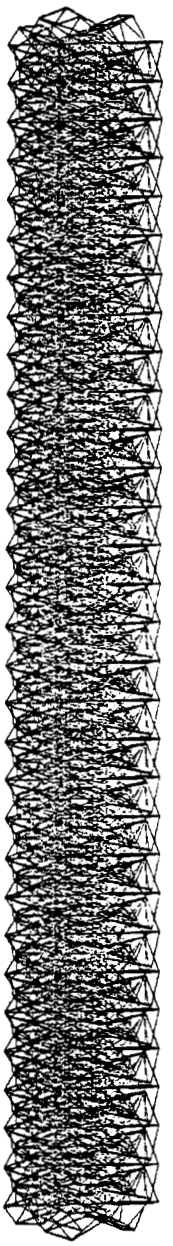

Fig. 5.5. NASTRAN model of seven-strand wire rope without end mass.

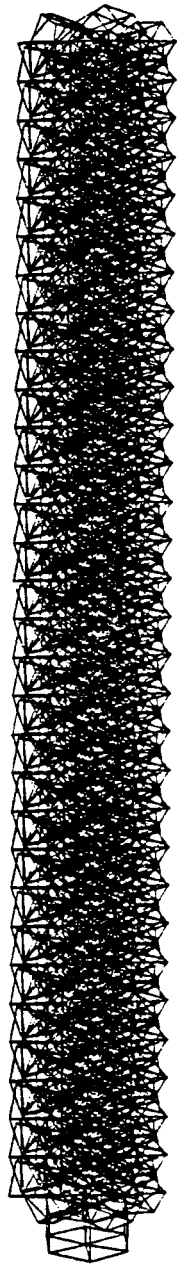

Fig. 5.6. NASTRAN model of seven-strand wire rope with end mass.

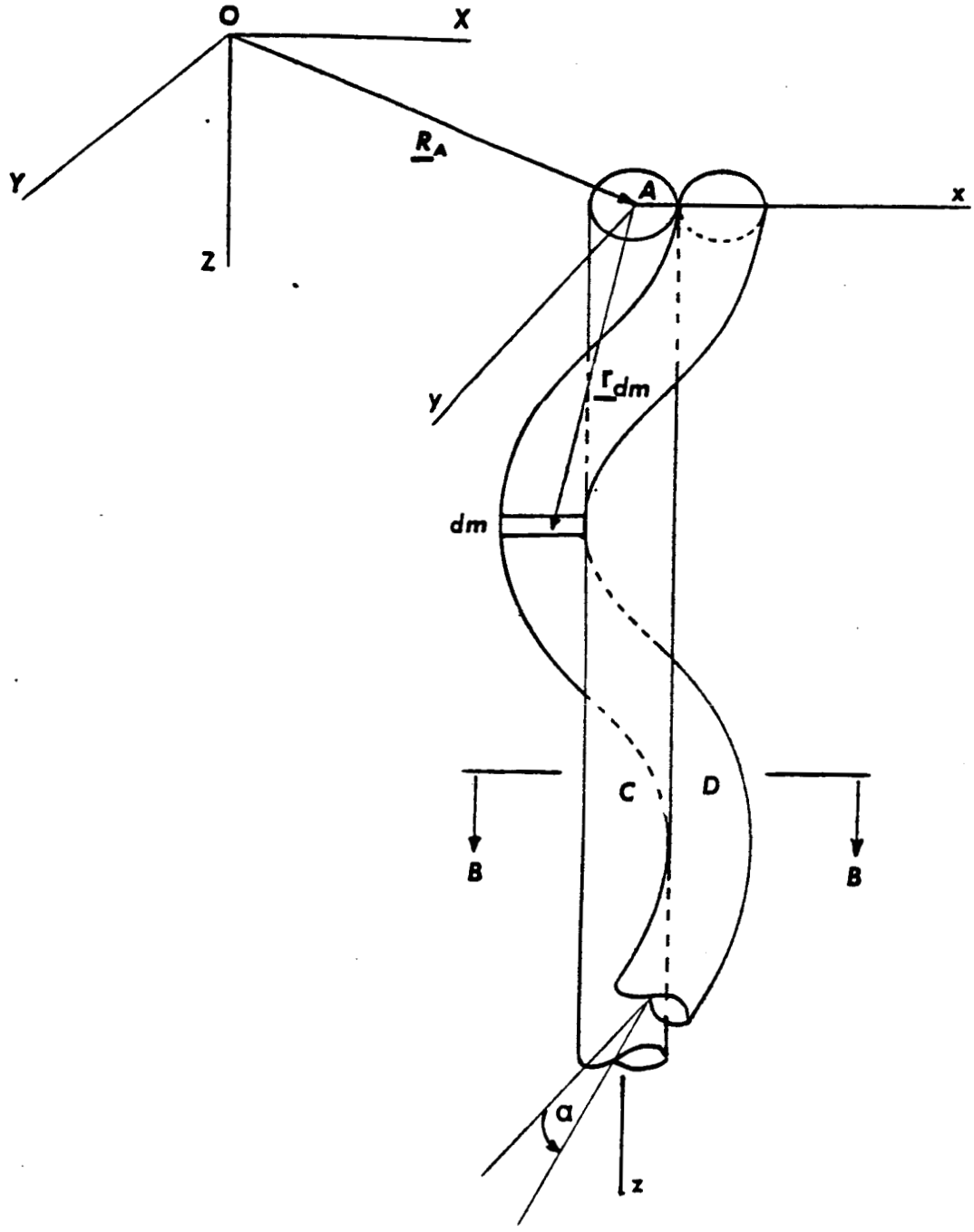

Fig. 5.7. Two-strand wire rope.

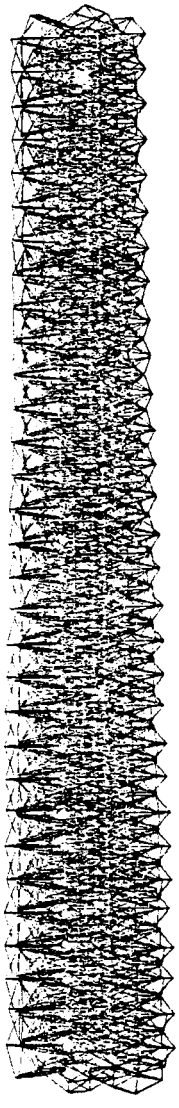

Fig. 5.8. Typical mode shape showing end separation (no end mass).

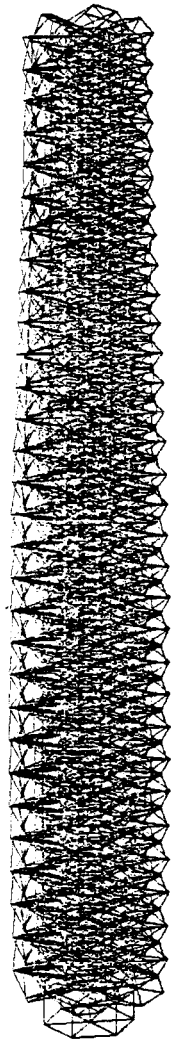

Fig. 5.9. Typical mode shape showing end separation (with end mass).

Fig. 5.10. Typical mode shape showing slipping between strands.

APPENDIX A. ISOLATOR SHAKER TESTS

A comparison of the accelerations of the isolator base and the center mass is shown in Fig. A-1 and the displacements of the mass and the base are shown in Fig. A-2. Isolator transmissibility and effectiveness as functions of frequency are shown in Figs. A-3 and A-4 respectively. Transmissibility is defined as the ratio of mass displacement to base displacement, and isolator effectiveness is defined as one minus transmissibility. While the behavior shown in these figures may not seem atypical to that of other vibration isolation systems, Fig. A-2 shows a displacement much like that of materials with high loss factors (see pp. 133-134 of Nashif, et al. (1985)) or beneficial damping (see pp. DDD-3 and DDD-16 of Rogers (1984).

Figure A-1

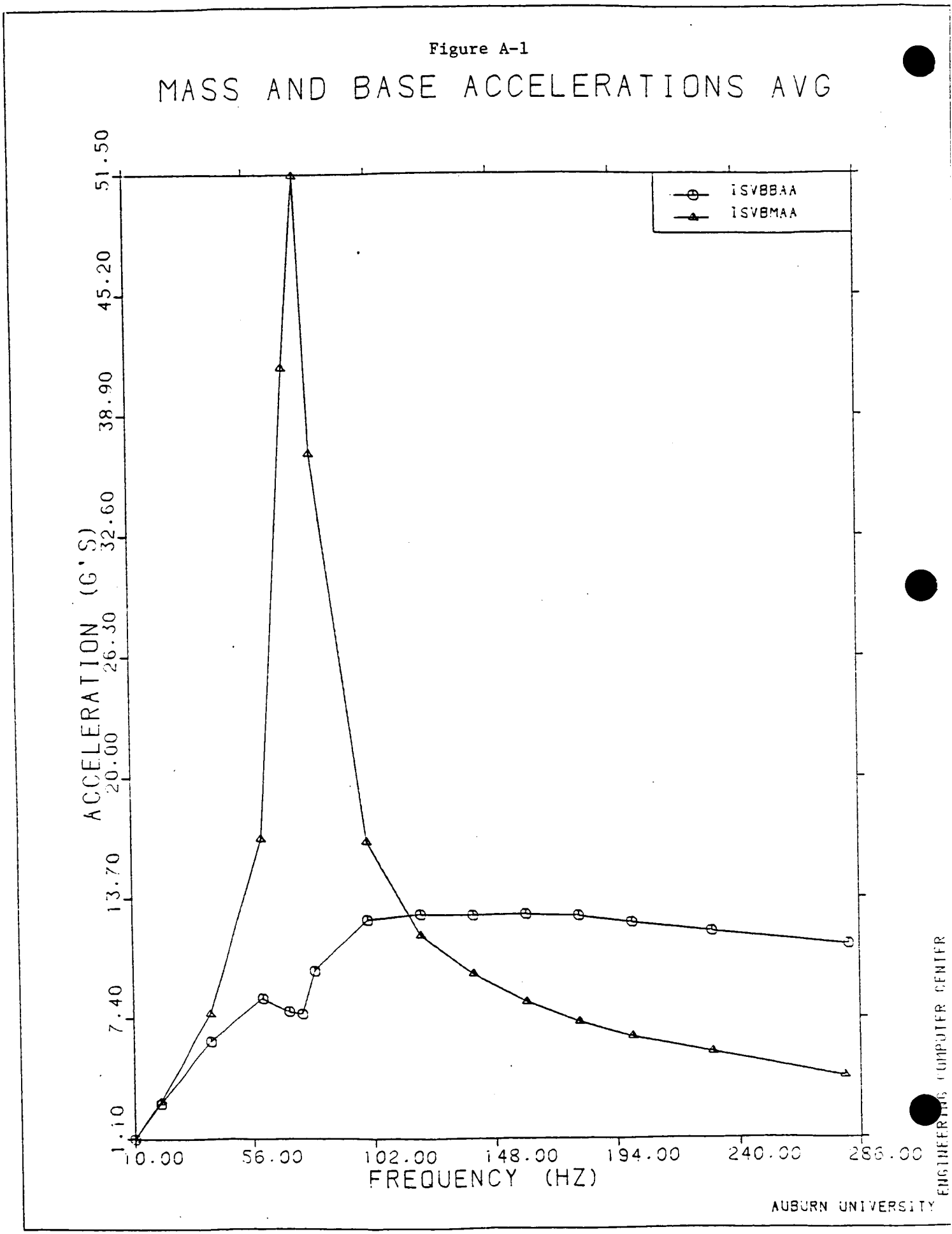
MASS AND BASE ACCELERATIONS AVG
ISVBBAA
ISVBMAA
ACCELERATION (G'S)
51.50
45.20
38.90
32.60
26.30
20.00
13.70
7.40
1.10
10.00
56.00
102.00
148.00
194.00
240.00
286.00
FREQUENCY (HZ)
AUBURN UNIVERSITY
ENGINEERING COMPUTER CENTER

Figure A-2

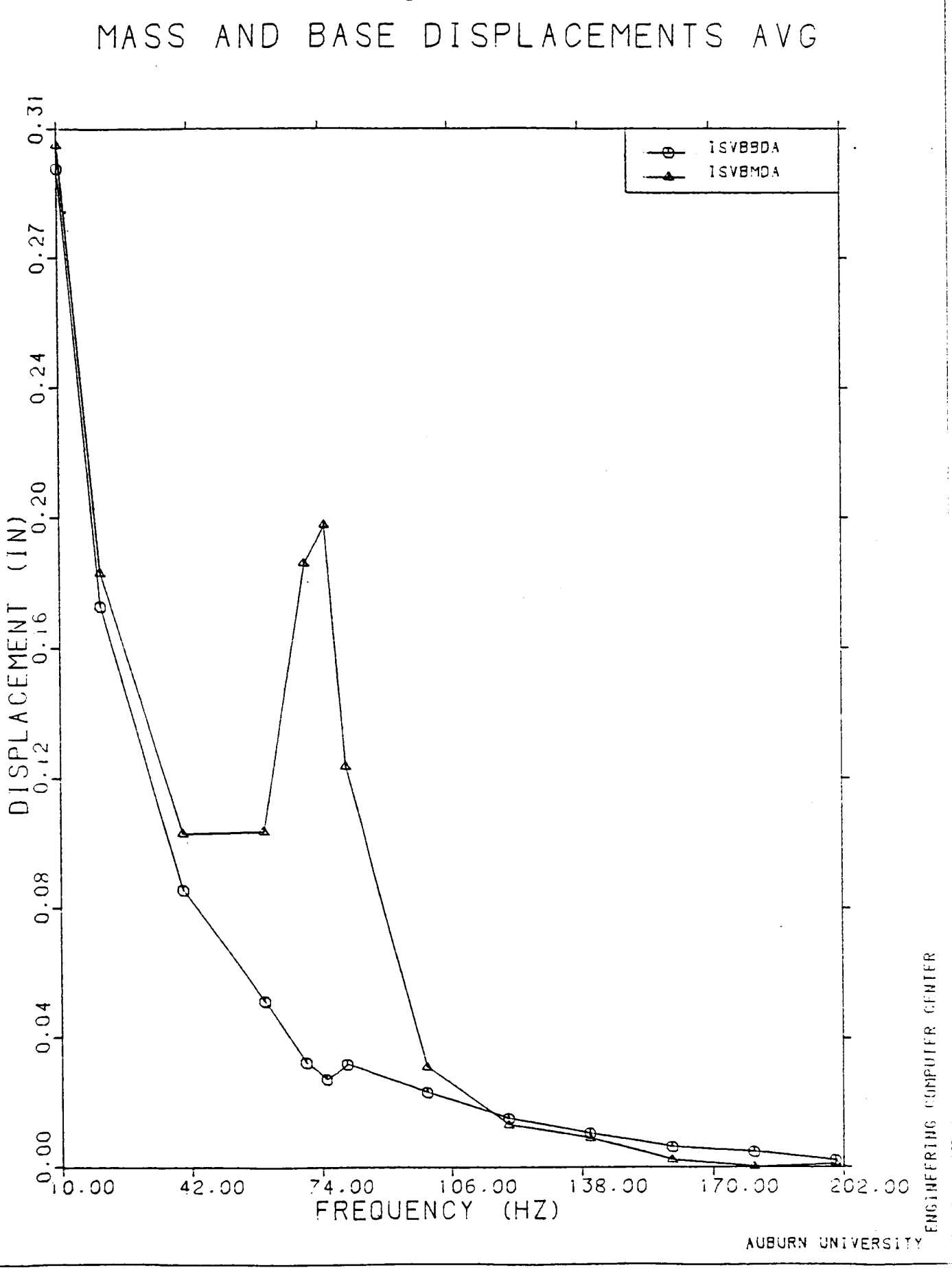
MASS AND BASE DISPLACEMENTS AVG
ISVBBDA
ISVBMDA
DISPLACEMENT (IN)
0.00
0.04
0.08
0.12
0.16
0.20
0.24
0.27
0.31
10.00
42.00
74.00
106.00
138.00
170.00
202.00
FREQUENCY (HZ)
AUBURN UNIVERSITY ENGINEERING COMPUTER CENTER

Figure A-3

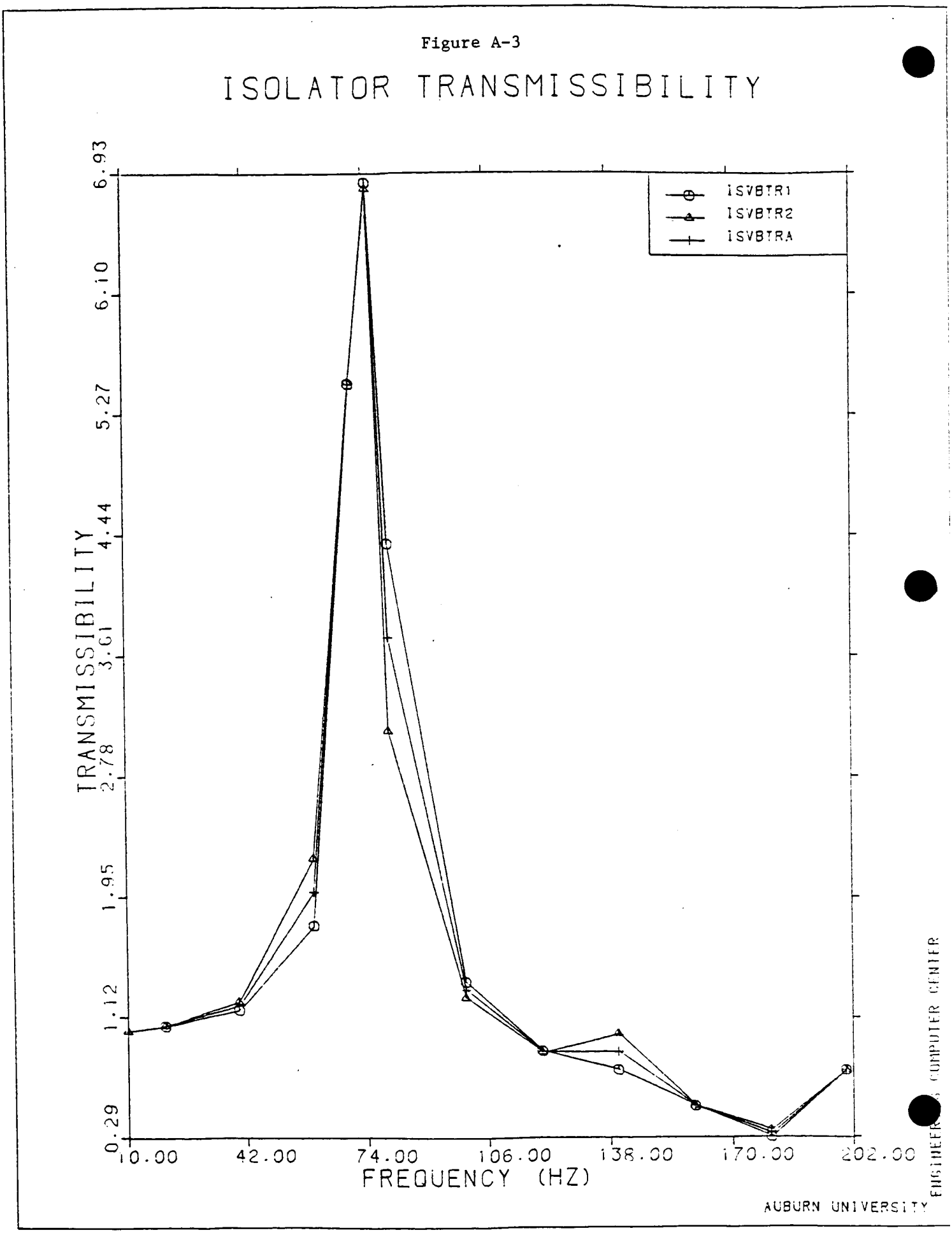
ISOLATOR TRANSMISSIBILITY
ISVBTR1
ISVBTR2
ISVBTRA
TRANSMISSIBILITY
0.29
1.12
1.95
2.78
3.61
4.44
5.27
6.10
6.93
10.00
42.00
74.00
106.00
138.00
170.00
202.00
FREQUENCY (HZ)
AUBURN UNIVERSITY
ENGINEERING COMPUTER CENTER

Figure A-4

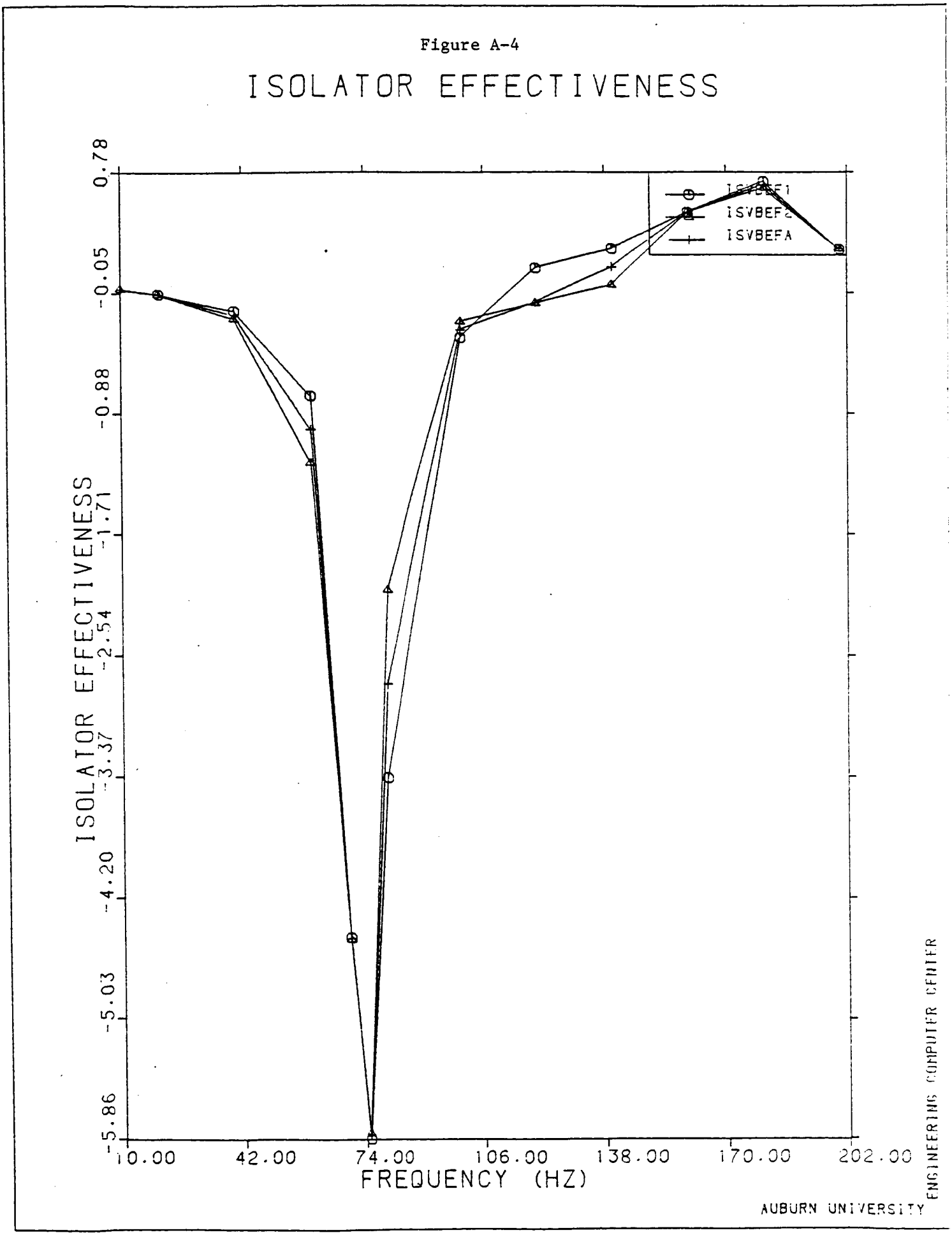
ISOLATOR EFFECTIVENESS
ISVBEF1
ISVBEF2
ISVBEFA
ISOLATOR EFFECTIVENESS
0.78
-0.05
-0.88
-1.71
-2.54
-3.37
-4.20
-5.03
-5.86
10.00
42.00
74.00
106.00
138.00
170.00
202.00
FREQUENCY (HZ)
AUBURN UNIVERSITY
ENGINEERING COMPUTER CENTER

APPENDIX B. WIRE ROPE PROPERTIES

The area moments of inertia used in this NASTRAN model are found by using I for a circle of radius r for each wire making up the wire rope in combination with the parallel axis theorem. For six strands plus a core strand,

$$I_x = 7\ I_c + [\pi r^2(2r)^2]2 + [\pi r^2(r^2)]4 = \frac{55\pi}{4}\ r^2 \qquad \text{(B.1)}$$

It can be shown that <u>any</u> orientation of the axes yields the same result. For the cable used in the experimental arrangement (one with a non-fibrous core), Eq. (B.1) yields

$$I_x = I_y = 1.04293 \times 10^{-5}\ \text{in}^4 \qquad \text{(B.2)}$$

where r = D/6 and D = 0.133 in. The polar moment of inertia is given by

$$J = I_x + I_y = 2.085 \times 10^{-5}\ \text{in}^4 \qquad \text{(B.3)}$$

Various areas were calculated, based on different assumptions, but were found <u>not</u> to affect the stiffness calculated from the NASTRAN output.

Increased confidence in the static results from the model is anticipated prior to extensive dynamic runs of the model; however, various schemes for including damping in the NASTRAN model and for producing the resulting hysteresis loops have been initiated.